Environmental Science and Pollution Research (2025) 32:5551–5573
https://doi.org/10.1007/s11356-025-35884-9

RESEARCH ARTICLE

Polymeric organic *Amberlite™ IRC-200* extract resin compound as a novel corrosion inhibitor for carbon steel in 1.0 M HCl acid: detail experimental, surface, molecular studies (DFT + MC/MD) and kinetic isotherm adsorption

Jaouad Bensalah[1] · Abdelfettah Hmada[1] · Said Bouzakraoui[1] · Nadia Dkhireche[1] · Abdelkader Zarrouk[2,3] · Şaban Erdoğan[4] · Burak Tüzün[5] · Nuha Wazzan[6] · Zaki S. Safi[7] · Hamid Erramli[8] · Mohamed Ebn Touhami[1] · Amar Habsaoui[1]

Received: 25 March 2024 / Accepted: 30 December 2024 / Published online: 11 February 2025

Abstract

The potential adsorbent for inhibitors of corrosion in HCl 1.0 M was investigated using experimental and modeling data on a novel cationic polymeric resin composite called *Amberlite™ IRC-200*. The resin has a significantly better ability to adsorb the Ni(II) ions. Molecular dynamics (MD), scanning electron microscopy (SEM), Fourier transform infrared spectroscopy (FTIR), X-ray diffraction (XRD), and DFT theory were among the methods used to examine the polymeric adsorbent resin. In this work, the adsorbent cationic polymeric resin is used to suppress corrosion in HCl 1.0 M. Experimental results demonstrated that ACQ and DAQ significantly increased MS corrosion resistance; results from Tafel polarization demonstrated that resin polymeric compounds exhibited disordered-type inhibitory properties with varying corrosion rates. Results from the highest best impedance experiments showed that at 100 ppm, ACQ inhibited performance to a 94.9% degree. Adsorption of the cationic adsorbent polymeric resin followed the most recent findings in the Langmuir model, and the most recent estimations of thermodynamic parameters indicated physisorption. Scanning transmission electron microscopy was used to investigate the MS morphological investigation.

Keywords Adsorption resin · *Amberlite™ IRC-200* polymeric · Mild steel corrosion · SEM/IR/EDS/XRD · DFT/MC/MD

Introduction

Inorganic material's continuous impairment pending exposure to an aquatic environment-containing agent is corrosive. Damage to the economy, threats to national security, and pollution

Responsible Editor: Philippe Garrigues

✉ Jaouad Bensalah
Jaouad.bensalah@uit.ac.ma

[1] Laboratory of Advanced Materials and Process Engineering, Department of Chemistry, Faculty of Sciences, Ibn Tofaïl University, B.P. 133, 14000 Kenitra, Morocco

[2] Laboratory of Materials, Nanotechnology and Environment, Faculty of Sciences, Mohammed V University in Rabat, P.O. Box. 1014, Rabat, Morocco

[3] Laboratory of Industrial Engineering, Energy and Environment (LI3E), SupMTI, Rabat, Morocco

[4] Department of Nutrition and Dietetics, Faculty of Health Sciences, Yalova University, Yalova, Turkey

[5] Plant and Animal Production Department, Technical Sciences Vocational School of Sivas, Sivas Cumhuriyet University, Sivas, Turkey

[6] Chemistry Department, Faculty of Science, King Abdulaziz University, P.O Box 42805, 21589 Jeddah, Saudi Arabia

[7] Chemistry Department, Faculty of Science, Al Azhar University-Gaza, P.O Box 1277, Gaza, Palestine

[8] Team of Materials, Electrochemistry and Environment (LCOCE), Department of Chemistry, Faculty of Sciences, Ibn Tofail University, BP 133, 14000 Kenitra, Morocco

are only some of the outcomes of this degeneration (Abbou et al., 2022). Corrosion prevention in inorganic materials is an advanced topic that has attracted the interest of a large group of specialists in the field (Bensalah et al. 2023a, b). Mild steel (MS) is a combination of iron (Fe) with an idealistic presence of up to 0.29% in order to increase its intensity and fracture resistance compared to other forms of iron (Fe) metal (Abiola and Tobun 2010). It is all because people cannot get enough of metals. Its inexpensive price and appropriate mechanical capabilities have led to its widespread use, which in turn has contributed greatly to human civilization's progress (Zhou et al. 2023). Damage and wear to the morphology of ion metals and retrogradation of the integrity of their elemental compositions are experienced by equipment retrieved from the MS that comes into touch with a corrosive aquatic environment (Bentiss et al. 2003). This, in turn, impacts productivity and longevity. Hence, it is critical to protect the MS from corrosion. Utilizing inhibitors of corrosion is a powerful tool in the fight against corrosion, since it is both impact- and user-friendly and offers protection against corrosion. Organic corrosion inhibitors that adhere to idealistic principles have heteroatoms, electron-donating groups, a cycle structure, and conjugated bonds (Ben Hmamou et al. 2012; Rouifi et al. 2020; Zarrouk et al. 2012; Zhong et al. 2023). The organic inhibitors were studied by forming a barrier film against the cantankerous solution (Sherif et al. 2008). Such self-assembling frequently films contain chemical or physical shape adsorption processes (Schafferman et al. 1998). Diverse organic families of compounds have largely been used to limit corrosion inorganic, particularly in media acidic (Tayebi et al. 2014).

The resin *Amberlite*™ *IRC-200* polymeric is an important molecular motif in order to unique characteristics such as activities biological and properties luminescent (Kayadibi et al. 2016). Analytical chemists often employ the polymeric resin *Amberlite*™ *IRC-200* for the complexation of different metals, and even hydrometallurgists can use it to precipitate ions of metal (Ouakki et al. 2020). Lately, some that the adsorbent resin polymeric containing in the developed as inhibitors of corrosion for the various ions metals in order to of the attraction of the sites adsorptive (Schafferman et al. 1998). The sodium 4-(sec-butyl) benzenesulfonate resin adsorbent *Amberlite*™ *IRC-200*. The high presence of a too-short distance between the phosphoric (=S) and oxygen (=O) groups renders that sodium 4-(sec-butyl) benzenesulfonate resin adsorbent cationic *Amberlite*™ *IRC-200* polymeric was an exemplary candidate for inhibitor corrosion. Studies have seen that modification of the resin adsorbent *Amberlite*™ *IRC-200* polymeric was moiety by the different substituents introduced at the various positions can enhance activity anticorrosion—200 polymeric derivatives can easily chemically or physically adsorb at the ion metal morphology in a solution aggressive (Naseri et al. 2018).

Organic surface morphology in a solution-aggressive environment refers to the study of surface features, structures, and behaviors of organic materials (such as polymers, biomaterials, or organic coatings) when exposed to harsh chemical environments. These environments are typically referred to as "aggressive" because they contain substances (like acids, alkalis, salts, or solvents) that can degrade, corrode, or otherwise alter the material's surface (Murulana et al. 2016). The most objective study of the research current is to moreover study the effective inhibition of the adsorbent resin polymeric-impregnated *Amberlite*™ *IRC-200* polymeric, which was on the (MS) study corrosion in solution 1.0 M HCl. The various conventional methods are experimental, including mass loss and electron scanning microscopy (SEM).

The present work deals with the adsorption and characterization of a resin polymeric compound namely *Amberlite*™ *IRC-200* (*AIRC-200*) and its application as a carbon steel corrosion inhibitor in 1 M HCl at 1500 rpm hydrodynamic state. The standard methods were used to explore the inhibitive performance of the resin. The estimation of the resin adsorption over the carbon steel surface was evaluated using scanning electron microscopy (SEM), EDS, and spectroscopie infrarouge (FTIR). The atomistic level inhibitive performance was screened by density functional theory (DFT) and molecular dynamic simulation (MD).

Material and methods

Material of the cationic resin Amberlite™ IRC-200

The sorbent material that was used in this work to attitude the adsorption technic of the used resin exchange *Amberlite*™ *IRC-200* polymeric CAS: 177-03729/2018, where the latter is a type of cationic resin containing the nomenclature presented chemical sodium 4-(sec-butyl) benzenesulfonate as follows in (Table 1).

The HCl (97%) solution and NaOH used to fix the pH of the metallic solution Ni $(NO_3)_2$ $(H_2O)_6$ which is the source of Nickel ions, the latter exploited to fix the ionic strength in aqueous solution. All solutions are prepared with distilled water, and its properties (physical and chemical) are seen in Table 1. An acrylic polymer microporous is utilized as an artificial adsorbent exchange cationic adsorbent resin polymeric in the synthetic route in the form of beads. Said polymeric resin was brought into adsorption contact with 1.0 M HCl, and then over rinsed cycles, several were washed with water distilled to purify the cationic support adsorbent and make it neutral.

Electrochemical technical measurements

Experiments of party electrochemical study have been performed utilizing a radiometer potentiostat analytical present

Table 1 The composition chemical of the *Amberlite™ IRC-200* adsorbent resin polymeric

Products	Aspect	Structure	Molar mass study (g mol^{-1})
Resin polymeric ***Amberlite ™ IRC-200***		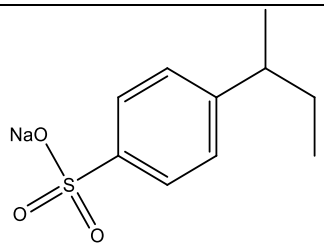	
Unhydrated Nickel nitrate		$Ni(NO_3)_2(H_2O)_6$	290.81

of the type PGZ 100. To obtain reliable results, we used Master Volta 4 software, controlled by an operator using an electrochemical computer associated with a cell comprising three electrodes, presented as a borosilicate glass (Pyrex™) cylinder. Close by a plug with three electrodes: equilibrium electrode calomel (*Amberlite™ IRC-200*), counter as a platinum electrode (Naseri et al. 2018), and MS study as samples electrode working that cut an MS with a cross-zone syllabic of 1 unity simple of the cm^2 study and embedded in a holder Teflon. It is immersed in 1M HCl electrolyte solution in the absence and presence of different inhibitor concentration at 298 K (Kouadri et al. 2018), In a open circuit, the potential stabilises and then reaches a certain level.

Scanning electron microscopy

Experiments of party electrochemical study have been performed utilizing a radiometer potentiostat analytical present of the type PGZ 100. To direct positive, utilized Master Volta 4 software which is controlled by an individual with a coupled electrochemical computer technically (Bensalah et al. 2022), the cell containing 3. In order to estimate the experimental results, the morphology surface of the micrographs present study according to perceived scanning microscopy electrons. Washed resin samples of metal ion Ni(II) are sunken in 1.0 M/HCl acid in the various steps of the presence metal Ni(II) and most presence marbles of the adsorbent resin polymeric for 6 h at room T(K). The SEM was used for various images obtained from surface micrographs made with a JEOL JSM-5500 microscope.

DFT details

DFT/B3LYP (Kadiri et al. 2018) approach with the 6–311 + G(d,p) level of theory in aqueous solution as implemented in Gaussian 09 software (Issa et al. 2010) was performed to optimize the geometries of the extracted *Amberlite™ IRC-200* resin in the ground states. The polarized continuum model (PCM) of solvation was used to model the optimization procedure (Li et al. 2011). Two species, which are the anion and protonated forms. The SCF density convergence = 1.0×10^{-6}, and the max SCF iterations = 300. The structures obtained were confirmed as minima to the potential energy surface, with no imaginary frequencies, by performing Frequency calculation at. To guarantee that the structure is minimal to the potential energy surface, an identical level of theory was used (no imaginary frequencies were found). In energy levels of the most filled and least filled molecular orbitals (E_{HOMO} and E_{LUMO}), GaussView was used to visualize the output file, and the results were extracted (Krishnegowda et al. 2013) which were then used to calculate the energy gap ($\Delta E = E_{LUMO} - E_{HOMO}$). The possible interaction of electrons during the donation and/or acceptance of an electron leads to the rearrangement of all orbitals and not just the occupation of the LUMO orbital or removal from the HOMO orbital. Therefore, the Kohn–Sham orbital, with the ionization potential and electron affinity as the negative eigenvalues of the HOMO and LUMO, respectively, does not give good results (Asan et al. 2006). Instead, the vertical ionization potential (VIP) and vertical electron affinity (*VEA*) were calculated using the following equations:

$$V_{IP} = E_0^+ - E_0$$
$$V_{EA} = E_0^- - E_0 \quad (1)$$

where E_0 is the total energy of the optimized structure and E_0^+ and E_0^- are, respectively, the energies of the cationic and anionic radicals at optimized geometries of the neutral structure. To compute the VIP and V*EA*, two single-point calculations using the same level of theory were performed for cation and anion radicals at the optimized structure of the neutral species (Krishnegowda et al. 2013).

At the optimal structure of the neutral species, the energies of the cationic radical, $E_0{}^+$, and the anionic radical, $E_0{}^-$, are equal to E_0. Absolute electronegativity (χ), global hardness (η), softness (σ), electrophilicity (ω), and the electronic effect of feedback (back donation is followed by the electronic energy ($\Delta E_{b\text{-}d}$) were computed using the following formulas to characterize chemical reactivity:

$$\chi = \frac{VIP + VEA}{2} \quad (2)$$

$$\eta = \frac{VIP - VEA}{2} \quad (3)$$

$$S = \frac{1}{\eta} \quad (4)$$

$$\omega = \frac{\chi^2}{2\eta} \quad (5)$$

$$\Delta E_{b-d} = -\frac{\eta}{4} \quad (6)$$

The chemical reactivity descriptor's findings are summed up in Table 1.

Monte Carlo simulations

In order to investigate potential metal interactions for leaching systems, Monte Carlo simulations have developed into a powerful computational tool (Cruz et al. 2004). These calculations were performed in the program Materials Studio 6.0 using the COMPASS (Condensed-phase Optimized Molecular Potentials for Atomistic Simulation Studies) force field. In this work (De Proft et al. 1996), metal atoms were selected as the metal to interact with the molecule. For the bond (E_{Bond}) of metal on every conceivable metal surface, the following formula was used:

$$E_{Bond} = E_{total} - (E_{0ChCl} + E_{Mn+}) \quad (7)$$

where E_{total} is the total energy of the simulation system after removing the water molecules, E_{surface} is the energy of the molecule, and is the energy of metal. Through a systematic exploration of different adsorption configurations, the equilibrium adsorption configuration, characterized by the least energy, was successfully identified, aligning with prior research findings. To enhance the inhibitory efficacy of inhibitor molecules and understand their preferred adsorption sites, obtaining this vital information was deemed essential. The research focused on the uppermost stratum of the Fe(110) interface due to its particular relevance to inhibitor adsorption. The methodology described facilitated a precise simulation of the adsorption process, incorporating the simulated cell's dimensions and a variety of corrosive species. The study yielded noteworthy results regarding the interaction between the inhibitor and the metallic surface, contributing to the development of corrosion prevention methods. Subsequently, the widely recognized COMPASS II force field was applied, and molecular dynamics (MD) simulations were conducted using the Forcite module in Materials Studio at a temperature of 298 K. During the MD simulations, all iron atoms (110) were immobilized, except for the two uppermost levels, spanning a simulation duration of 0.800 ns with a time step of 1.0 femtoseconds. To enhance comprehension of the inhibitor molecule's adsorption properties on the metal surface, the radial distribution function (RDF) was computed using MD simulation trajectories (Bensalah et al. 2022). Monte Carlo calculations were conducted through temperature cycling, ranging from 10^5 to 10^2 K over ten cycles, each consisting of 100,000 steps. This process allowed us to obtain the lowest possible energy configurations at reduced temperatures, employing the same energy convergence criteria and force field as those used in the MD calculation.

Results and discussion

Characterization

The various images of the EDS and the SEM analysis

Figure 1a shows the morphology of the cationic adsorbent *Amberlite™ IRC-200* polymeric, and Fig. 1b shows the resin polymeric after acid cleaning. Both images are presented in Fig. 1. Figure 1a shows the results of the scanning electron microscopy (SEM) examination of the polymer resin *Amberlite™ IRC-200*, which shows that the surface of this cationic polymer resin contains numerous pores. This suggests that the chemical composition of this resin is not uniform, which is good for the resin.

Figure 1 shows the two scanning electron micrographs (SEM) of the polymeric resin *Amberlite™ IRC-200* before and after rinsing with hydrochloric acid (HCl) (Fig. 1). Figure 1 shows micrographs of the adsorbent polymeric resin *Amberlite™ IRC-200*. These micrographs reveal that the surface of the raw cationic resin polymeric *Amberlite™ IRC-200* has several micro-cavities, which suggest that the resin

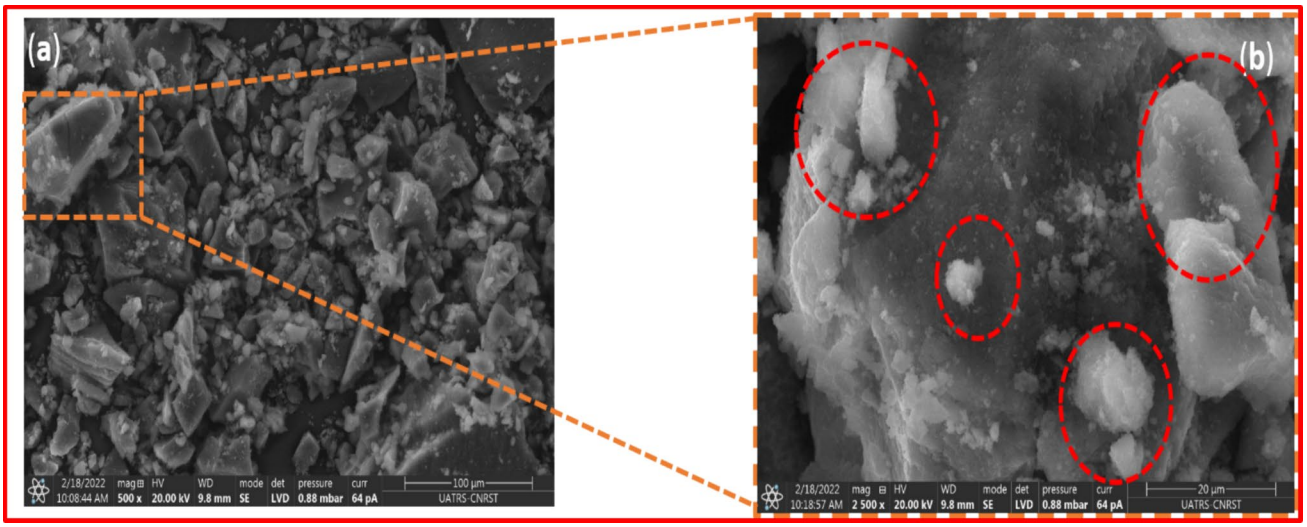

Fig. 1 The scanning electron micrographs (SEMs) of the polymeric adsorbent *Amberlite™ IRC-200*, which is cationic, show **a** the results of the HCl treatment research and **b** the combined effect of the two chemicals

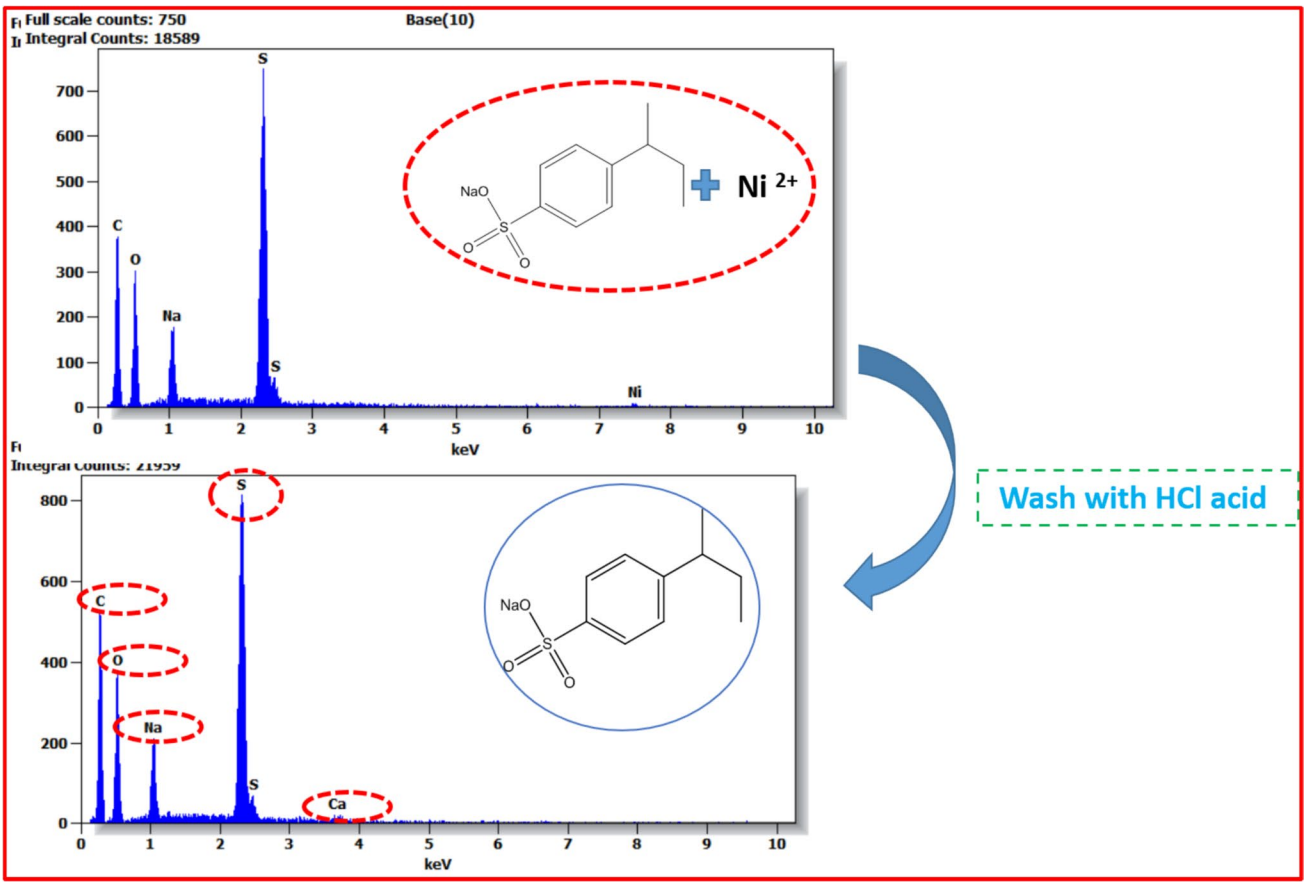

Fig. 2 The different images EDS of the cationic resin polymeric in pellet form (*Amberlite™ IRC-200*) before brute and after cleaning with HCl (*Amberlite™ IRC-200* + HCl)

is advantageous for adsorbents due to its many pores and disordered molecular structure.

The various EDS graphs (Fig. 2) signalize the presence of metal, initially which exists in the cationic *Amberlite*™ *IRC-200* polymeric resin worn. The acquired spectrum following the washing of HCl acid on the cationic *Amberlite*™ *IRC-200* (Fig. 2) presents a considerable peak that represents the chlorine after the reaction of complexes with the ions of chloride.

Spectroscopies FTIR

Figure 3 shows the adsorbent cationic *Amberlite*™ *IRC-200* polymeric brute before and after washing with HCl acid, and the chemical composition of the two materials was limited using Fourier technical spectroscopy transformation infrared.

The cationic adsorbent *Amberlite*™ *IRC-200* polymeric processed with the acid present washed with HCl solution acid dominated the spectral analysis due to the distinct chemic features of the various vibration bands.

Pictured above is the spectrum of the polymeric cationic adsorbent *Amberlite*™ *IRC-200* before it was cleaned with a solution of HCl for FTIR analysis. See that the signal intensity of the C-H band was triggered by strip bonds at 3312 cm^{-1}. These high bands present at 1716 cm^{-1} and 3464 cm^{-1} confirmed S = O. The different characteristic chemic bands present of the various constituents of water that are displayed above 1663.00 cm^{-1} also another band present around vibration 1706.00 cm^{-1} signalized the two bonds following present (C–C/S–O). The band stretch an 1153.00 cm^{-1} of S–O shown in Fig. 3 seems to be larger and stronger than that of cationic *Amberlite*™ *IRC-200* resin polymeric before washing with acid HCl.

Mechanism of Ni(II) adsorption

Depending on the metal type and the cation resin used, the mechanisms of metal adsorption might be quite complex. The study found that out of all the processes examined, ion exchange had the greatest impact on the efficiency and effectiveness of cationic resin. It was previously believed that the ion exchange change process was malleable and that HCl acid washing could recover a significant amount of the adsorbed metal (Dane et al. 2007). By studying the

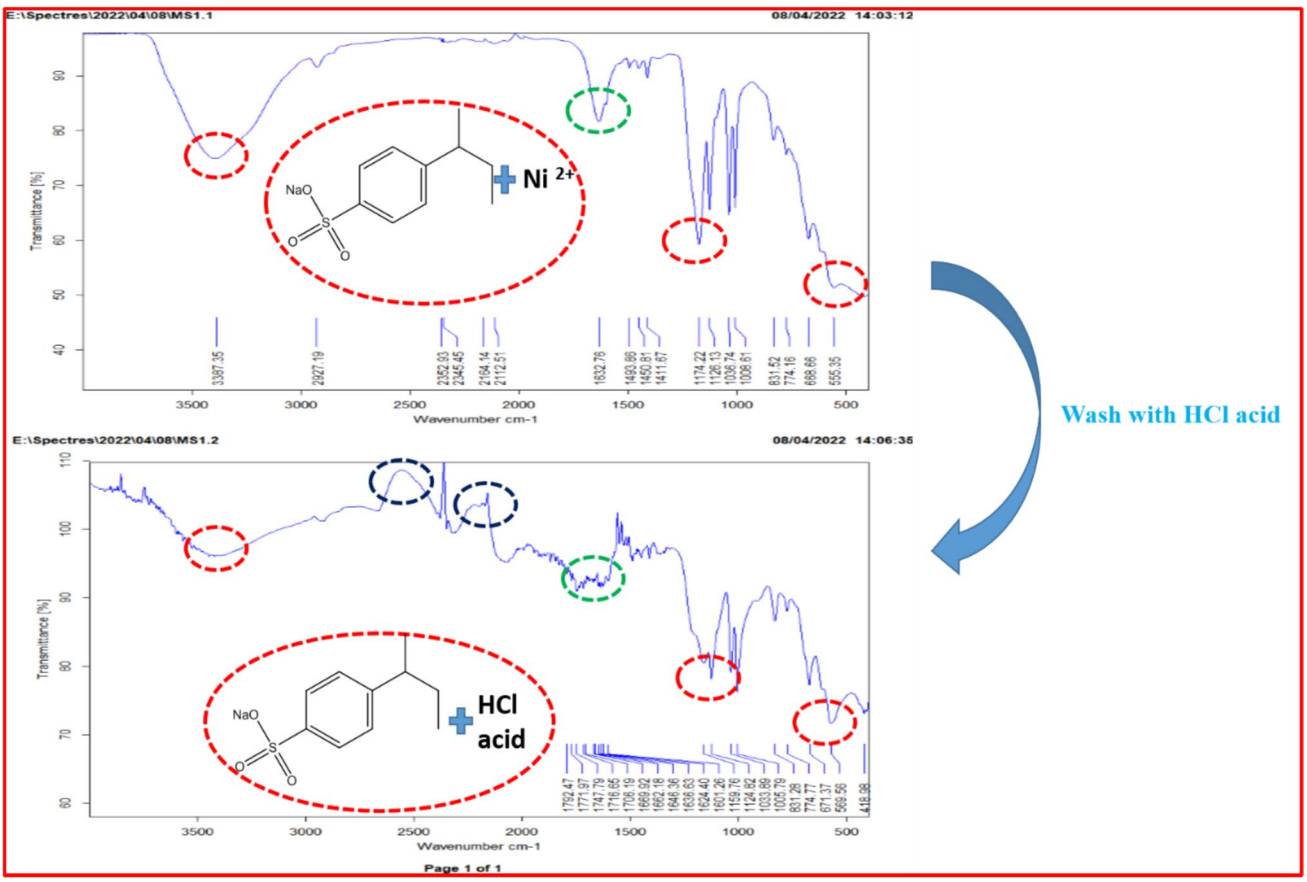

Fig. 3 The various spectra present, which are obtained by infrared analysis (FTIR) of the *Amberlite*™ *IRC-200* unwashed and *Amberlite*™ *IRC-200* after washing with HCl acid

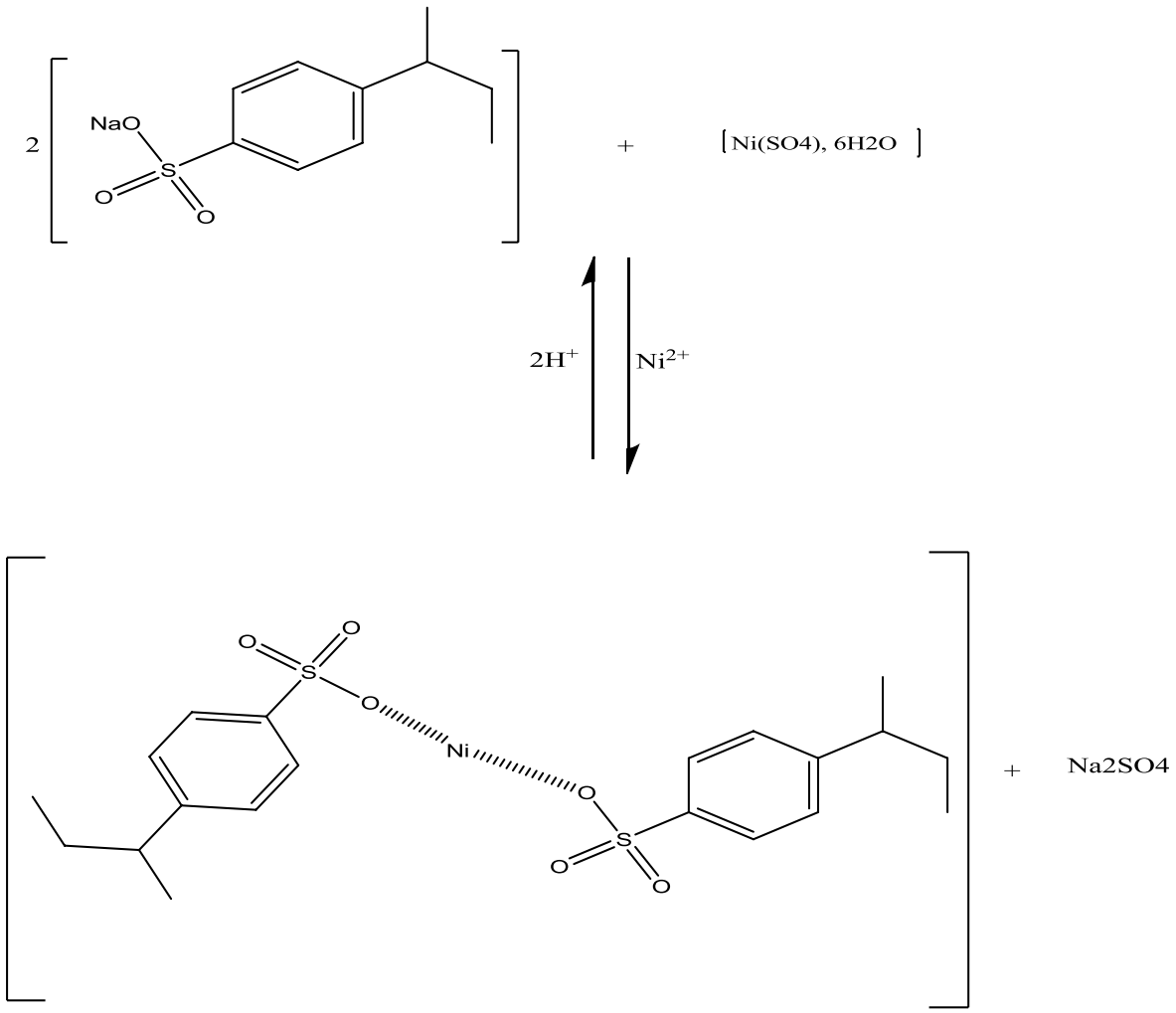

Fig. 4 Possible mechanisms of the cationic adsorbent polymeric of Ni(II) by both types of adsorption

sorption of Ni (II) on our the cationic resin in the presence of basic pH can be adsorbed for the resin it conclude that the bond are strong and that the mechanism involved and chemisorption and that the mechanism of complexation is always accompanied by an exchange of ions in this case Ni (II) reacts with ketones and/or amines groups present on the surface of the cationic polymer that in exchange release a proton H+. The resin also contains hydrophobic zones (around the carbon atoms) which have some influence on the overall properties, including solubility Fig. 4.

The porous walls of many cationic resins were composed of a solid and amorphous matrix; also, their composition study was organic polymer (Jiménez-Sánchez et al. 2023). The cation resin has a wide variety of functional groups, all of which have the potential to aid in the adsorption of Ni(II) metal and the utilization of complexometry. Based on the findings of this morphological investigation of the organic polymer, oxygen and phosphonate groups were identified (Issa et al. 2010). Notably, it was brought to light that the presence of an exploited group does not constitute a singular technical process and that identical functional groups can be involved in many mechanisms. The investigation of oxygen atoms was linked with complexation with nickel(II), in addition to ion exchange (Hu et al. 2016), while the phosphate was found to be complex with the metal Ni(II) (Hsissou et al. 2021). The adsorption mechanism study's determination may, therefore, be inaccurate if it is based solely on the functional groups supplied by the cation resin. Prior findings established that the ion exchange mechanism, which involves the oxygen group on the cation resin, was responsible for the adsorption of Ni(II) metal (Ho et al. 2009).

Impacts of concentration of Amberlite™ IRC-200 on the efficiency inhibition and the corrosion

Stationary electrochemical study part

The Tafel model of polarization presented curves for the MS present in 1.0 M HCl acid solution without and with

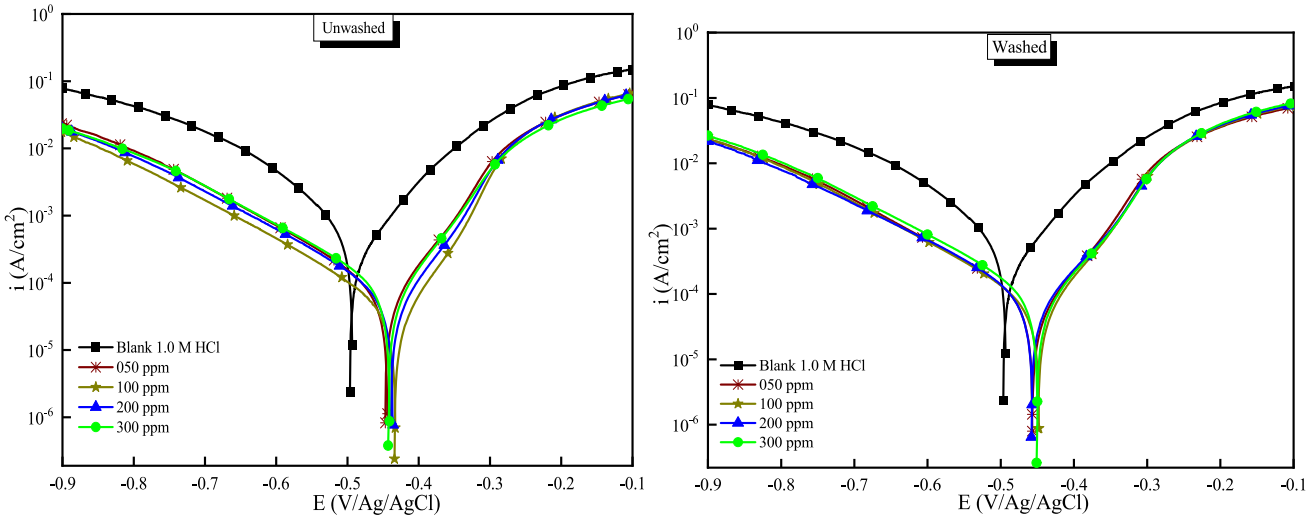

Fig. 5 Tafel model of polarization presented for the steel present in solution HCl/1.0 M: washed and unwashed with the different concentrations study of adsorbent exchange polymeric resin at 298 K

Table 2 Electrochemical of the presenting parameters for MS present in 1.0 M solution HCl solution with the presenting concentrations study of the resin *Amberlite™ IRC-200* cationic polymeric at 298 K

Medium	Conc. (M)	E_{corr} (mV/Ag/AgCl)	i_{corr} (μA cm^{-2})	β_c (mV dec^{-1})	β_a (mV dec^{-1})	η_{PP}%
1.0 M HCl	–	−498	983	140	150	———
Unwashed	50 ppm	−444	85	135	101	91.4
	100 ppm	−432	46	132	89	95.3
	200 ppm	−437	68	134	94	93.1
	300 ppm	−441	96	145	105	90.2
Washed	50 ppm	−456	88	138	102	91.0
	100 ppm	−447	74	130	98	92.5
	200 ppm	−456	84	137	101	91.5
	300 ppm	−449	99	139	104	89.9

different concentrations studied as 50 ppm, 100 ppm, 200 ppm, and 300 ppm of the adsorbent exchange cationic *Amberlite™ IRC-200* resin polymeric at 298 K are seen in Fig. 5.

The various electrochemical parameters present the Tafel constant of cathodic (β_c), Tafel constant of anodic (β_a), current corrosion density (i_{corr}), potential corrosion (E_{corr}), and the efficiencies inhibition corresponding η_{pp} illustrated in Table 2.

Inhibition efficiency values were calculated using Eq. 8, where η represents the inhibition efficiency:

$$\eta_{pp}(\%) = \frac{i_{corr} - i_{inh}}{i_{corr}} \times 100 \tag{8}$$

The corrosion current densities (i_{corr} and i_{inh}) were calculated in micro-ampere per square centimeter by extrapolating the cathodic and anodic Tafel lines to the corrosion μA cm^{-2} potential both before and after the addition of the inhibitor.

It seemed cathode to be more clear and the intensity present corrosion of supplements diminution compared safely to the space, as shown in Fig. 6 and Table 2, because both the catholic and anodic reactions were affected in high most presence by the various presenting concentrations study of the resin polymeric *Amberlite™ IRC-200* cationic inhibitor. This remarkable technological development of the organic inhibitor on the washed side in HCl acid has altered the major presence in the Tafel slopes of the two electrodes, the anodic (a) and the cathode (c). The presence of the adsorbent polymeric resin allows for this observation. In parallel, we get the discordant together with the anodic/cathode in unwashed polymeric in acid HCl solution acid of the polymeric cationic adsorbent *Amberlite™ IRC-200* resin. The diminution in the process of corrosion can be explicated by together metal dissolution and the development of the various hydrogen bonds at the ion inorganic surface due to the phenomenal process of the various organic compounds

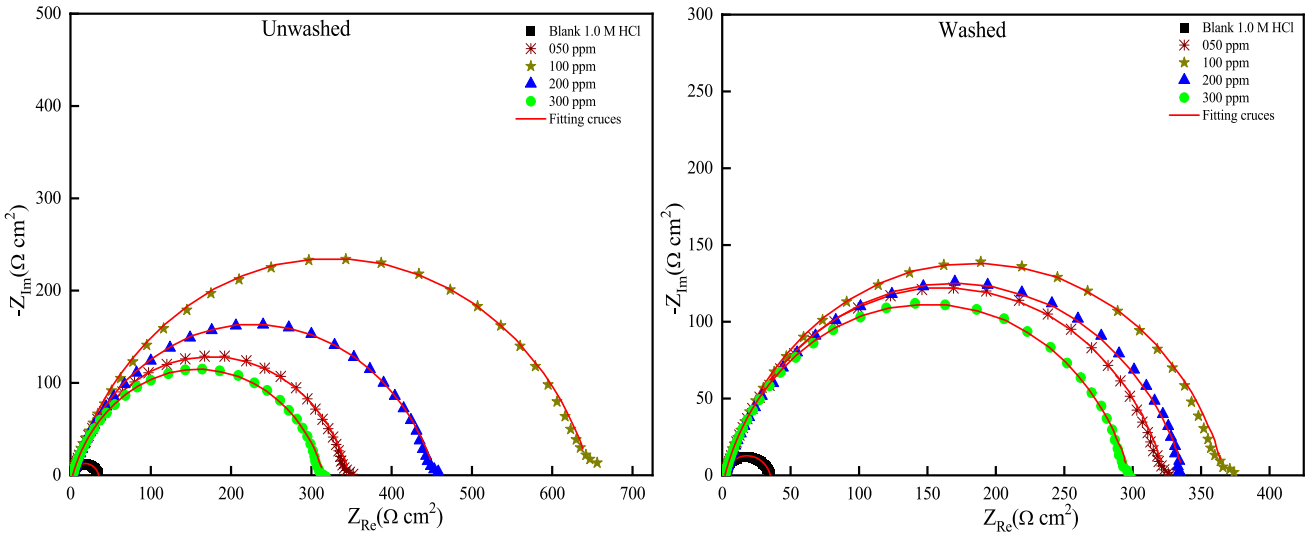

Fig. 6 The various diagrams impedance for MS in HCl solution: washed and unwashed with the various concentrations present of adsorbent polymeric at 298 K

studied (Lu and Chen 2012) present in the adsorbent resin cationic polymeric *Amberlite*™ *IRC-200* on the high morphology of the MS study. These cationic rings' organic or double present bonds in polymeric compound study act as an inhibitor of the type mixed, and the phenomenal inhibition process is a cause to the mechanism study engineering (Ghazoui et al. 2014). The parallel cathodic Tafel lines and slight variations in β_c in Fig. 5 suggest that the cathodic process, or hydrogen evolution reaction, exhibits sensitivity to regulated activation. Initially, inhibitor molecules adhere to the steel surface, thereby obstructing the reactive sites from engaging in reactions. Consequently, less surface area is available for H^+ ions, yet the fundamental mechanism of the reaction remains unchanged (Khaled 2003). The β_a values decreased with both inhibitors' incorporation, pointing to the inhibitors' influence on the anodic reaction (ElBelghiti et al. 2016). This demeanor implies the shaping of a shielding coating due to inhibitor molecules adsorbing onto the steel surface, lessening the active sites on it.

The various obtained results in 1.0 M HCl acid containing a solution of 100 ppm of *Amberlite*™ *IRC-200* cation polymeric resin at 298 K signalized a decrease in the corrosion current density of the MS from 96 to 99 µA cm^{-2}. This attitude can be elucidated by good encasement of the metal surface by *Amberlite*™ *IRC-200* resin polymeric particles that prevent the various sites from active on the ion's metal morphology (Hegazy et al. 2014). The decrease in corrosion current density due to the two inhibitors results in an enhancement in charge transfer resistance, hence decelerating the anodic and cathodic processes.

Finally, from all these obtained results experimentally, it is explicit that this resin *Amberlite*™ *IRC-200* polymeric extract has the best adsorbent inhibitory for the corrosion process of the steel light in a medium acidic solution of unwashed adsorbent polymeric.

Impedance part

The impact of the adsorbent resin polymeric effectuated concentration by the plots of the Nyquist for steel light in 1.0 M HCl solution in washed and unwashed at 298 K as shown in Fig. 6.

The various models present, Bode plots, and Nyquist study of both simulated and experimental data of the iron MS in 1.0 M HCl solution with and without 100 ppm of the cationic *Amberlite*™ *IRC-200* polymeric resin are shown in Fig. 7.

The Bode plots and Nyquist of both simulated data and experimental MS study in wash and unwashed solution with and without the various concentrations of the resin of the cationic resin *Amberlite*™ *IRC-200* are seen in Fig. 8. Based on the two representations in Fig. 7, the equivalent electrical circuit is shown in Fig. 8 used to best model the presence of the interface-MS/solution. It is clear that the plots' impedance is best in accordance with those different calculated studied by the used equivalent present model circuit.

The generality of the obtained curves of impedance for this technical corrosion is present in MS in 1.0 M HCl solution acid, within the first as washed and unwashed of HCl acid, with this consist of inhibitor study of two exploited capacitive loops. The different loops increased with increasing concentration of the inhibitor study,

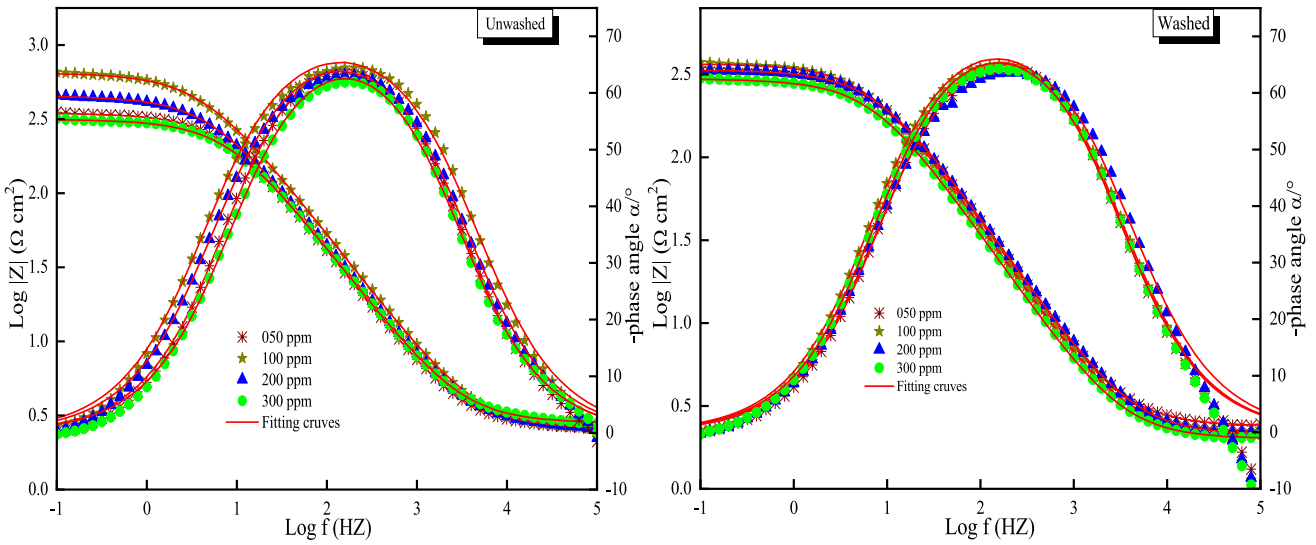

Fig. 7 Bode plot for MS in 1 M HCl with washed and unwashed without and with different concentrations of the resin *Amberlite™ IRC-200* polymeric at 298 K

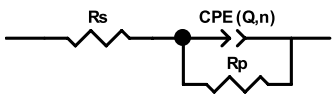

Fig. 8 Electrical equivalent exploited circuits for this modeling study of the interface of MS in 1.0 M HCl solution

indicating that the surface area covered by the *Amberlite™ IRC-200* adsorbent increases with increasing concentration of the *Amberlite™ IRC-200* polymer resin. The high presence of two various capacitive loops is attributed to the technical obtained relaxation by the type adsorption like Cl^-/H^+ on the surface electrode study (Dagdag et al. 2020).

Equation 9 defines the impedance of the CPE (Z_{CPE}) in the equivalent circuit, taking into account the CPE exponent (n) that reflects the inhomogeneity or roughness of the electrode surface (Behpour et al. 2008).

$$Z_{CPE} = Q^{-1}(i\omega)^{-n} \tag{9}$$

Equation 10 describes the calculation of the double-layer capacitance (C_{dl}) based on the impedance data obtained. Equation 11 calculates the inhibition efficiency (η) based on R_p values with and without inhibitors.

$$C_{dl} = \left(Q \times R_p^{1-n}\right)^{1/n} \tag{10}$$

$$\eta_{imp}(\%) = \frac{R_p - R_p^o}{R_p} \times 100 \tag{11}$$

The impedance parameters obtained from fitting analyses of EIS profiles are presented in Table 3, which includes the

Table 3 The different parameters of impedance for mild steel in 1.0 M HCl with different concentrations presented in this adsorbent study *Amberlite™ IRC-200* cationic polymeric at 298 K

Medium	Conc. (ppm)	R_s (Ω cm^2)	R_p (Ω cm^2)	Q (μF s^n cm^{-2})	n_{dl}	C_{dl} (μF cm^{-2})	θ	η_{imp} (%)
1.0 M HCl	–-	1.12	34.7	419	0.773	120.9	—-	—-
Unwashed	50 ppm	2.575	344.9	129	0.805	60.7	0.8993	89.9
	100 ppm	2.497	646.8	108	0.799	55.3	0.9463	94.9
	200 ppm	2.568	451.9	125	0.815	65.1	0.9232	92.3
	300 ppm	2.805	312.8	131	0.797	58.1	0.8890	88.9
Washed	50 ppm	2.382	321.0	125	0.825	63.2	0.8993	89.2
	100 ppm	2.168	365.4	114	0.829	59.2	0.9463	90.5
	200 ppm	2.095	335.6	120	0.815	57.9	0.9232	89.7
	300 ppm	1.992	295.5	143	0.823	72.4	0.8890	88.3

polarization resistance values with and without inhibitors, denoted as R_p and R_p^o, respectively. Table 3 summarizes the EIS parameters for mild steel in 1.0 M HCl, with and without varying concentrations of inhibitors.

In generality and with another study, that is possible behavior inductive at faint frequency due to the adsorption technical of the products corrosion on the high electrode presenting all the various obtained parameters in this experimentally from loops high amplitude. Is intelligible in this augmentation present in the different values of R_p, as rises study from 312.8 (Ω cm^2) to 646.8 (Ω cm^2), in parallel a diminution with the various values of C_{dl} from 131 (μF cm^{-2}) to 108 (μF cm^{-2}). In parallel, in the polymeric study washed with HCl solution and side (Dane et al. 2007), however, on the second step unwashed polymeric side with HCl solution, we detected a slight increase in different values of R_p, as rises from 321 (Ω cm^2) to 295.5 (Ω cm^2), with a simultaneous diminution in Q of the various values from 125 (μF s^n cm^{-2}) to 143 (μF s^n cm^{-2}) shown in Table 3. The increase in the double layer led thickness to a decrease in the various values of the C_{dl} determined which led to a diminution in the constant dielectric due to the segregation of the water-absorbed molecules chemic present of the adsorbent study (cationic polymeric) on the surface morphology of the MS study (Geethanjali and Subhashini 2015).

Therefore, in the obtained results of the technical polarization study and the EIS studies, it was observed that the efficiency inhibition increased with the concentration increase of the *Amberlite*™ *IRC-200* polymeric resin (Tables 3 and 4), the maximum reaching values of 94.9% and 89.9% to 88.9% for HCl solution acid unwashed and in parallel from 90.5 to 88.3%. For washed cationic polymeric adsorbent by HCl solution extracted from the *Amberlite*™ *IRC-200* polymeric in HCl solution, due to the augmentation adsorption of the inhibitor molecules to activate the various sites studied on this surface present in the MS study in the different conditions. The various effectiveness of the adsorbent resin *Amberlite*™ *IRC-200* polymeric is best compared to the studies previously scrutinized by the various other materials exploiting.

Table 4 The various study parameters of electrochemical for MS in HCl solution of the adsorbent *Amberlite*™ *IRC-200* washed and unwashed of acid HCl solution with the various T(K)

Medium	Temperature (K)	E_{corr} (mV/Ag/AgCl)	i_{corr} (μA cm^{-2})	β_c (mV dec^{-1})	η_{pp}%
Blank	298	−498	983	140	—
	308	−477	1200	184	—
	318	−487	1450	171	—
	328	−493	2200	161	—
Unwashed	298	−432	46	132	95.3
	308	−455	130	143	89.2
	318	−469	202	154	86.1
	328	−468	329	155	85.0
Washed	298	−447	74	130	92.5
	308	−470	146	144	87.8
	318	−474	260	153	82.1
	328	−471	410	147	81.4

Impact study of the temperature

Figure 9 presents the different curves indicating the polarization of the MS presence of the concentration 100 ppm of the resin adsorbent *Amberlite*™ *IRC-200* polymeric at different T(K) as 298, 308, 318, and 328 K in the medium study 1.0 M HCl solution.

The different values of potential (E_{corr}) present, the high current corrosion density (i_{corr}) obtained, the various slopes present β_c and β_a, and the efficiency inhibition (E%) are seen above (Table 4). The obtained efficiency inhibition is decreased with the increase of T(K) from 95.3 to 85.0% in the 1.0 M medium acid of the *Amberlite*™ *IRC-200* washed and from 92.5 to 81.4% for the cationic *Amberlite*™ *IRC-200* resin polymeric unwashed.

Thermodynamic party

Results from the thermodynamic party allow for a more precise quantification of the efficiency of inhibition studies conducted against corrosion, allow for the parameters present and the energy required for activation to be more precisely determined in thermodynamic party studies, and provide an explanation for the technical nature of the investigation used to uncover these results.

The Arrhenius curves (Fig. 10) and Arrhenius transition curves (Fig. 10) are plotted by the technical calculating of the method logarithmic of the various rates of corrosion (ln i_{corr}) with respect to (1000/T) and (ln i_{corr}/T) with respect to (1000/T), respectively, for medium acidic 1.0 M solution HCl shown in Fig. 10. The Arrhenius Eqs. (12) and (13) can be used to compute the thermodynamic activation parameters of steel in an acidic medium as a result of this study (Geethanjali and Subhashini 2015).

$$Ini_{corr} = \frac{-E_a}{RT} + InA \tag{12}$$

From Table 6 below, the E_a increases with the high addition study of the cationic adsorbent exploiting the *Amberlite*™ *IRC-200* resin polymeric over the solutions control are as follows. This change in the process corrosion rate study with the various temperature augmentations was studied in HCl (1.0 M) unwashed with HCl acid and washed with HCl acid solution, of the adsorbent study the *Amberlite*™ *IRC-200* polymeric resin

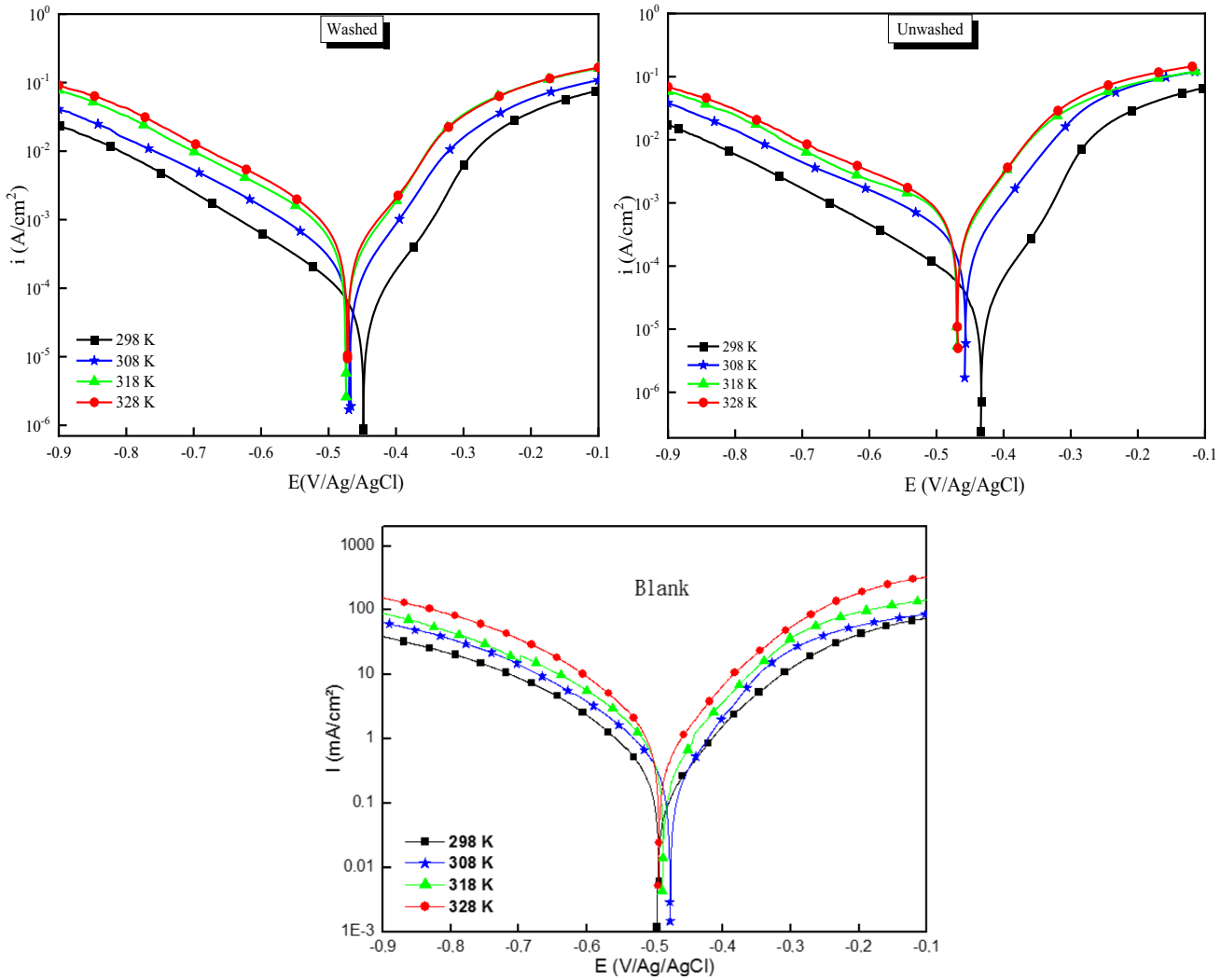

Fig. 9 Tafel polarization present curves for MS study in 1.0 M HCl solution in the absence (**a**) presence of the resin cationic ***Amberlite***™ ***IRC-200*** washed in HCl acid solution **(b)** and unwashed in HCl acid solution **(c)** and the presence of this adsorbent resin ***Amberlite***™ ***IRC-200*** cationic with the various T(K) present

of 100 ppm of the technical inhibitor process. Table 5 contains the various data received from the various curves next equation.

The increase in the technical corrosion process is seen with the augment for both HCl solutions in the absence of the resin polymeric *Amberlite*™ *IRC-200*. The rapid increase in the corrosion process is observed with increasing temperature in the absence of *Amberlite*™ *IRC-200* polymer resin, the addition of *Amberlite*™ *IRC-200* cation resin results in a rapid decrease in the corrosion rate.

$$In\left(\frac{i_{corr}}{T}\right) = \left[In\left(\frac{R}{hN_a}\right) + \left(\frac{\Delta S_a}{R}\right)\right] - \frac{\Delta H_a}{RT} \tag{13}$$

where R is the gas constant, T refers to the absolute temperature, N refers to Avogadro's number, h is Plank's constant, E_a is the activation corrosion energy, ΔH_a is the enthalpy of activation, and ΔS_a is the entropy of activation.

The various values of the energies this technical presents (E_a, $\Delta H_a/\Delta S_a$) are grouped jointly in Table 5. From high results obtained, it is prominent that high-value use of the energy enthalpy ΔH_a obtained from the next equation is 4.31 kJ mol^{-1} of adsorbent study polymeric resin washed by the solution acid and 4.82 kJ mol^{-1} of polymeric resin unwashed by HCl solution in the 1.0 M medium solution, which saw the endothermic process character of this technical process on the surface of the MS study.

The different value entropy is increased from – 61.66 J mol^{-1} K^{-1} on washed HCl solution acid and from – 46.95 J mol^{-1} K^{-1} on unwashed HCl solution; *Amberlite*™ *IRC-200* polymeric forms two distinct stages in an HCl solution medium with 100 ppm of inhibitor. This can be explained

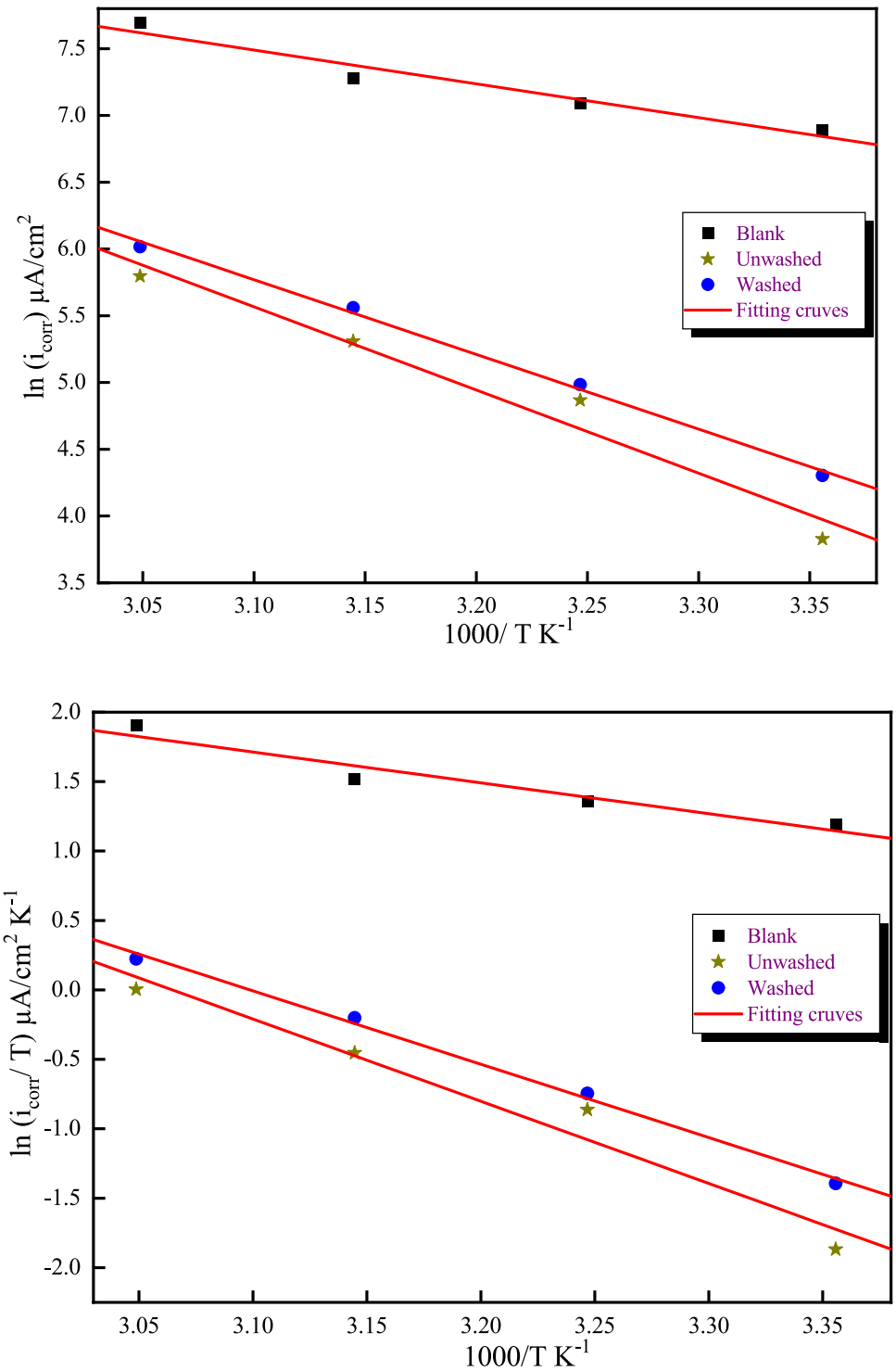

Fig. 10 The different Arrhenius curves corresponding to the corrosion of the steel in HCl acid, unwashed and washed of the adsorbent polymeric *Amberlite™ IRC-200*

Table 5 Activation of the parameters study for mild steel in acid HCl 1.0 M

Medium	E_a (kJ/mol)	ΔH_a (kJ/mol)	ΔS_a (J/mol K)
Blank	21.0	18.5	− 126.0
Unwashed	51.77	49.18	− 46.95
Washed	46.45	43.87	− 61.66

by the fact that the level of chaos increased just before the extract made contact with the steel in the experiment (Cruz et al. 2004). In parallel, when the molecules adsorbed on the surface morphology of the MS study, there will be a diminution in the unrest after a diminution in the value of entropy energy (Eidi et al. 2015).

Scanning electron microscopy (SEM)

Scanning electron microscopy (SEM) was used to examine the surface morphology of the MS after it had been immersed in a corrosive solution for 6 h in both washed and unwashed adsorbent resin *Amberlite™ IRC-200* (Fig. 11). To fill up the research and verify the findings from the electrochemical technical measures (EIS), we did this. These images demonstrate that after 6 h in HCl acid solution in the absence of the inhibitor, the morphological surface of the MS study is severely affected (Fig. 11). Corrosion has occurred uniformly across the steel in the absence of the (blank) inhibitor, as shown above. Steel submerged for 6 h in HCl solution adsorbent resin *Amberlite™ IRC-200* polymeric cationic plate shape, signaled the existence of the organic cationic at the substrate morphology based on surface morphology (Fig. 11). This experimental investigation demonstrates that the creation of an adsorbent, insoluble, and persistent organic coating inhibits corrosion by preventing the high electrolyte technical from penetrating the MS surface (Amri et al. 2022).

Energy-dispersive X-ray (EDX) analysis study

In order to comprehend the mechanism protection, EDX obtained from the steel morphology surface study was carried out after 6 h in the solution of HCl acid. The EDX obtained spectrum (Fig. 12 and Table 6). In the absence of inhibitors, the metal, carbon, and oxygen peaks were present, which is evidenced by the presence of inhibitors.

These crests reflect probably the existence of the metal oxide study. This is the result of the reaction complexation of the present steel.

In parallel, inhibitor levels drop when the researched factors are present. The concentration of oxygen as a percentage (Table 6) signalized the presence of phosphoric acid present, that is, the group initial of the chemical composition of the sorbent resin. These findings back up those from the carbon steel investigation, which showed that the protective film formed on the surface morphology of the latter, making it an exceptional corrosion inhibitor for the MS study in a 1.0 M HCl solution acid (Fuikui 1982).

DFT results

Global chemical reactivity

For the DFT study, two structures of the *Amberlite™ IRC-200* resin were considered. The first structure corresponds to the anion form in which the Na^+ ions are discarded from the structures, whereas the protonated form corresponds to the structure in which the anion form interacted with an acidic proton (Zarrouk et al. 2013). The proposed structures were

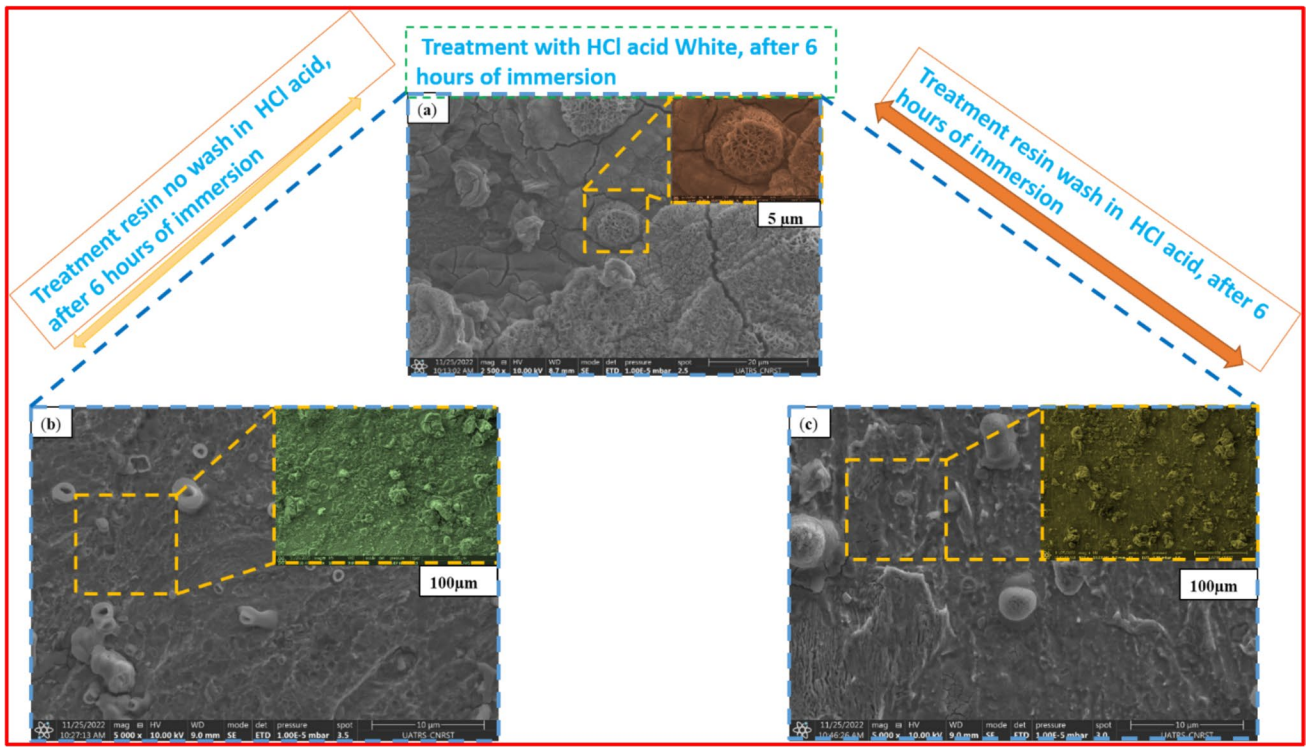

Fig. 11 The various pics SEM photomicrographs of the MS exploited in 1.0 M HCl with **a** untreated and **b** washed in presence acid study (HCl). **c** The adsorbent *Amberlite™ IRC-200* resin polymeric after 6 h of immersion

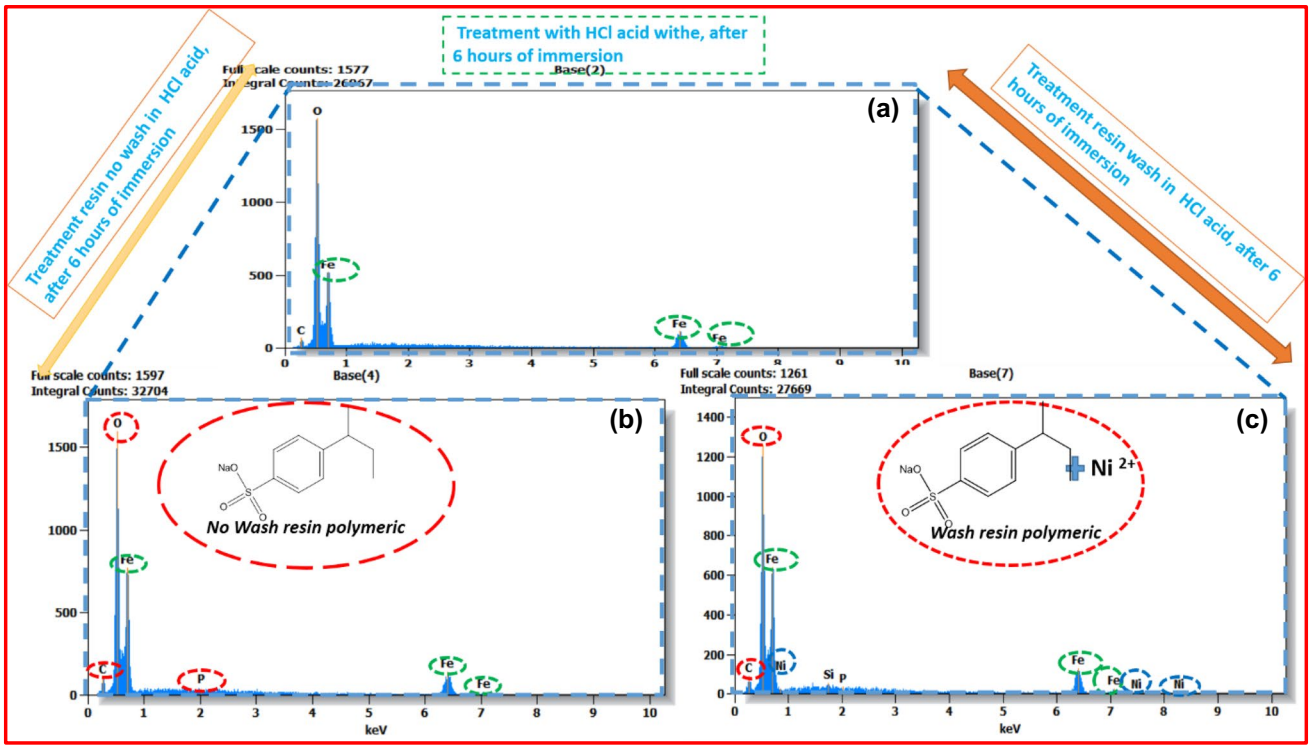

Fig. 12 The different EDX of the MS exploited in 1.0 M solution HCl with (**a**), untreated (**b**), and washed in the presence of HCl study (**c**) the adsorbent *Amberlite*™ *IRC-200* polymeric after 6 h of immersion

Table 6 The percentage mass study of the various elements obtained from the EDX obtained analysis of the morphology surface steel in the solution HCl acid of the adsorbent resin polymeric in washed and unwashed at $T = 298$ K

Elements	% Mass in blank of steel solution	% Mass in blank of steel solution with *Amberlite*™ *IRC-200* unwashed	% Mass of steel in blank solution with *Amberlite*™ *IRC-200* washed
C	35.3	11.6	19.2
O	1600.0	1530.0	1250.0
Ni	-	-	123.0
Fe	560.0	830.0	650.0

completely optimized in an aqueous solution according to the PCM solvation model at the B3LYP/6–311 + G(d,p) level of theory. Figure 13 shows the molecular structures, the distribution of the electron density HOMO and LUMO orbitals, and the electrostatic potential map of the anion and protonated forms of *Amberlite*™ *IRC-200* resin. The quantum chemical reactivity is summarized in Table 8. The LUMO surface is highly dispersed on the benzenesulfonyl moiety, while the HOMO surface is present throughout the inhibitor's whole moiety (Becke 1988). These findings show that the studied inhibitor is anionic due to its high electron-donating capability; this is supported by observing the anion's ESP map (Eidi et al. 2015). The ESP map of the anion is covered by red color, indicating that the electrons are delocalized and distributed over all molecules. On the other hand, the intensity of the red color is reduced in the protonated form due to the interaction of one of the oxygen atoms of the sulfonyl group with the acidic proton (Zarrouk et al. 2013).

For another qualitative view, the total density at HOMO and LUMO of the investigated species (TD-HOMO and

TD-LUMO) maps have been plotted using the same grid of color as shown in Figs. 14 and 15. The negative potential (strong red color) corresponds to the nucleophilic region of the molecule, which able to donate electrons to the metallic surface, whereas the positive potential (blue color) represents the electrophilic region of the molecule, which able to accept electrons from the metallic surface.

Strong contact between the HOMO and LUMO and, consequently, a high chemical reactivity are indicated by the relatively tiny values of the estimated energy gap of the inhibitor (anion 6.009 eV and protonated 5.877 eV) of the *Amberlite*™ *IRC-200* resin that can be detected. The results show that the energy gap of the protonated form is smaller than that of the anion form, suggesting that the inhibition efficiency of *Amberlite*™ *IRC-200* resin in an aqueous acidic solution is higher than that in a neutral aqueous solution. These results are also supported by computing the global chemical reactivity descriptors such as electronegativity,

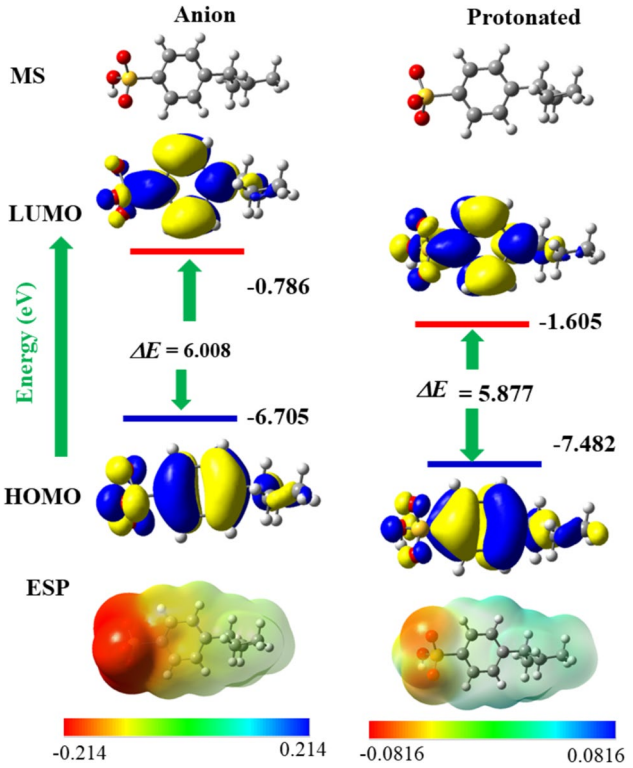

Fig. 13 The molecular structure (MS), the electron density distribution of HOMO and LUMO surfaces, and molecular electrostatic potential maps (ESP) of the anion and protonated forms of the *Amberlite*™ *IRC-200* resin. The energy diagrams are also depicted (energies in units of eV). The PCM solvation model is used for the calculations of the B3LYP/6–311 + G(d,p) level of theory

hardness, softness, and electrophilicity. Furthermore, the negative sign of the $\Delta E_{b\text{-}d}$ (Table 7). This takes into account how the tested inhibitor interacts with the steel surface and shows that *Amberlite*™ *IRC-200* resin is a good candidate for accepting electrons quickly (Kayadibi et al. 2016) and hence favored by the corrosion inhibition process.

Another important descriptor is the fraction of electron transfer during the inhibition process ($\Delta N1_{10}$), which is given by the following equation:

$$\Delta N_{110} = \frac{\Phi_{Fe} - \chi_{inh}}{2(\eta_{Fe}+\eta_{inh})} \tag{14}$$

where the $\Phi_{Fe} = 4.82eV$ is the work function of the Fe(110), the hardness of Fe, η_{Fe}= 0 eV, is taken as the assumption that for a bulk metal I = A because they are softer than the neutral metallic atoms (Doumane et al. 2023). ΔN_{110} should be lower than 3.6, and it shows the direction of the electron transfer during the adsorption process (El Kerdoudi et al. 2023). The positive value of the fraction of electron transfer suggests that the electron can flow from the *Amberlite*™ *IRC-200* resin to the steel surface, enhancing the electron flow process. The results in Table 7 found that the ΔN_{110} of the anion form (0.181) is higher than that of the protonated form (0.044), which is lower than 3.6 (Eidi et al. 2015).

The interaction strength between the HOMO and LUMO of the *Amberlite*™ *IRC-200* resin with the steel surface can be predicted by computing the energy gaps between the inhibitor and Fe surface by using the following equations:

$$\Delta E_1 = E_{LUMO}(inhibitor) - E_{HOMO}(Fe) \tag{15}$$

$$E_{LUMO}(Fe) - E_{HOMO}(inhibitor) \tag{16}$$

where the E_{HOMO} = 7.902 eV and E_{LUMO} = 0.151 eV are taken (Zarrouk et al. 2013). The data in Table 7 shows that both forms have $\Delta E_2 < \Delta E_1$ suggesting that the electron flow from the HOMO of the *Amberlite*™ *IRC-200* resin to the LUMO of the steel is energetically favored. In addition, the ΔE_2 of the protonated form is lower than that of the anion form, signifying that the interactions between the HOMO of the protonated form of the *Amberlite*™ *IRC-200* resin and the LUMO of the steel are stronger than that of the anion form.

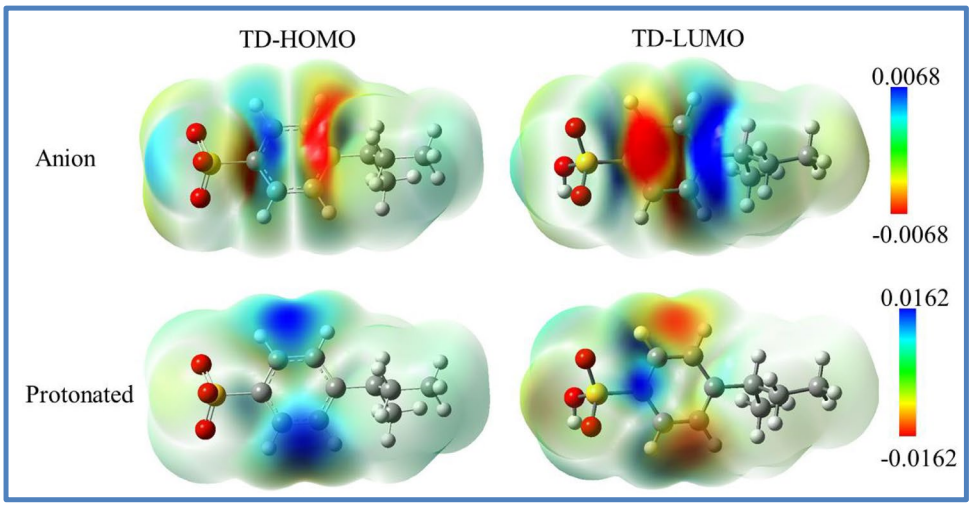

Fig. 14 Total densities at HOMO and LUMO (TD-HOMO and TD-LUMO) of the anion and protonated forms of the *Amberlite*™ *IRC-200* resin

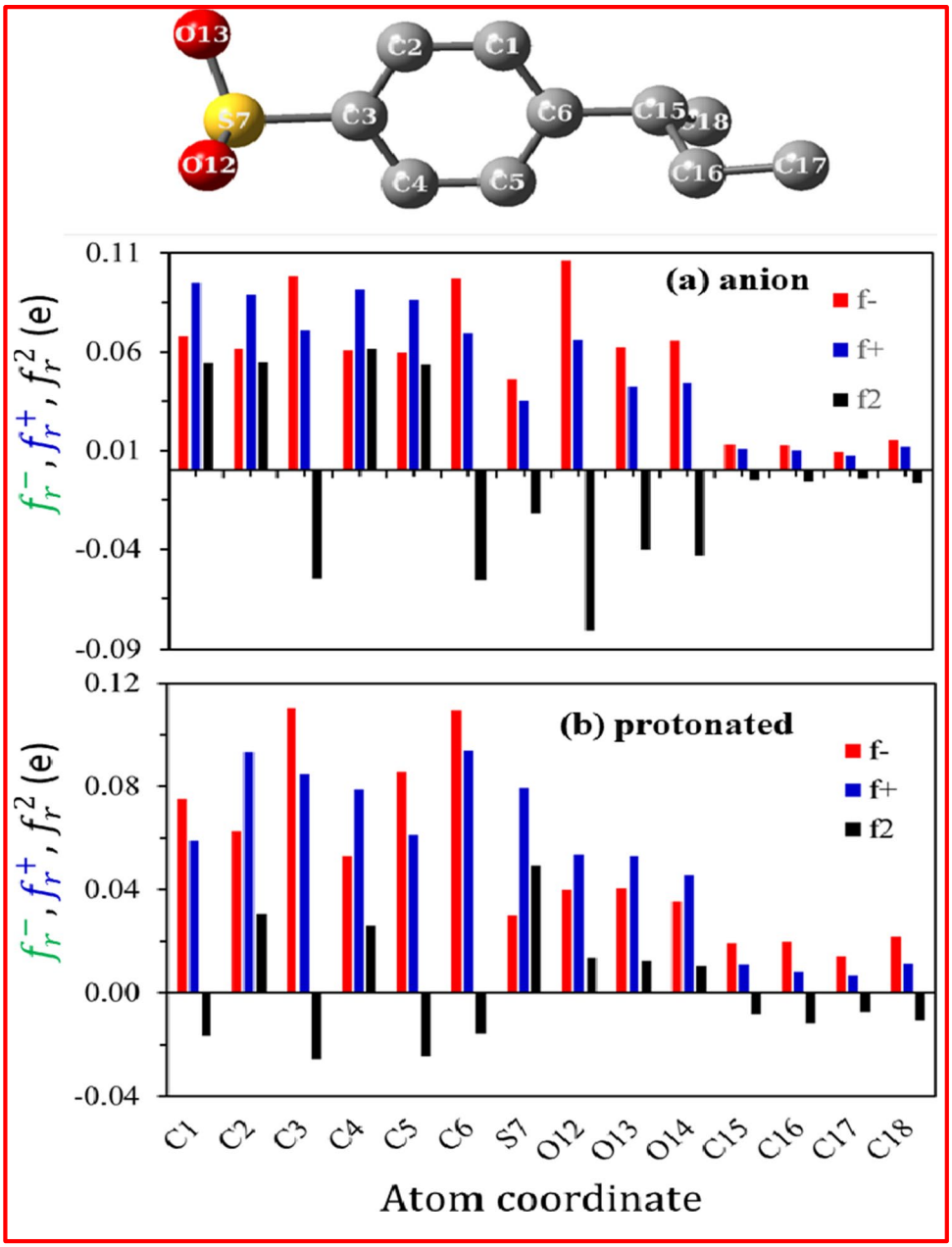

Fig. 15 Distribution of electrophilic and nucleophilic Fukui indices in a compact form (f_r^-, red columns), nucleophilic attacks (f_r^+, blue columns), and their dual descriptors (f_r^2, black columns) for anion (**a**) and protonated (**b**) forms of the *Amberlite*™ *IRC-200* resin at B3LYP/6–311 + G(d,p) in the PCM solvation model

Local reactivity

The local reactivity indices of the *Amberlite*™ *IRC-200* resin to decide in terms of Fukui functions for nucleophilic or electrophilous attacks have been calculated by using NBO analysis at the same level of theory for both inhibitors (Dkhireche et al. 2018). In order to accomplish this, the neutral (N), cationic (N-1), and anionic (N + 1) radicals of both inhibitors were analyzed, as well as their condensed Fukui indices, natural bonding orbitals, and natural population analysis. The following equations were used to determine the condensed Fukui functions for nucleophilic (f_k^+), electrophilic (f_k^-), and dual (f_k^2) attacks (Yadav et al. 2012):

$$\text{Nucleophilic attack} : f_k^+ = q(N) - q(N+1) \tag{17}$$

$$\text{Electrophilic attacks} : f_k^- = q(N-1) - q(N) \tag{18}$$

$$\text{Dual function} : f_k^2 = q(N+1) - q(N-1) \tag{19}$$

where $q(N)$, $q(N+1)$, and $q(N-1)$ are the Hirshfeld charges of the N, N + 1, and N-1 systems, respectively. The Fukui functions and their condensed values (Dane et al. 2007) were also visualized and calculated using the Multiwfn program (Dagdag et al. 2020). Figure 16 shows that the graph representation of Fukui indexes condensed

Table 7 Quantum chemical parameters of the *Amberlite*™ *IRC-200* resin calculated at the B3LYP/6–311 + G(d,p) level of theory in aqueous solution using PCM solvation model

Chemical parameters		Anion	Protonated
Total energy	E_0	−27,567.400	−27,579.176
Anion kinetic energy in neutral species geometries (eV)	E_0^-	−27,568.220	−27,580.921
Cation energy at neutral species geometries (eV)	E_0^+	−27,560.705	−27,571.780
The potential energy of the most filled molecular orbital (eV)	E_{HOMO}	−6.794	−7.482
The minimum occupied molecular orbital energy (eV)	E_{LUMO}	−0.786	−1.605
Energy gap (eV)	ΔE	6.008	5.877
Fe-inhibitor interaction	ΔE_1	7.117	6.297
Inhibitor-Fe interaction	ΔE_2	6.643	7.331
Vertical ionization potential (eV)	IP_V	6.695	7.396
Vertical electron affinity (eV)	EA_V	0.820	1.746
Fundamental gap	F_g	5.875	5.651
Electronegativity (eV)	χ	3.758	4.571
Hardness (eV)	η	2.938	2.825
Softness (eV^{-1})	S	0.340	0.354
Electrophilicity (eV)	ω	2.403	3.698
The fraction of electron transfer	ΔN_{110}	0.181	0.044
The back-donation energy	$\Delta E_{b\text{-}d}$	−0.734	−0.706
Dipole moment (Debye)	μ	21.0	8.2

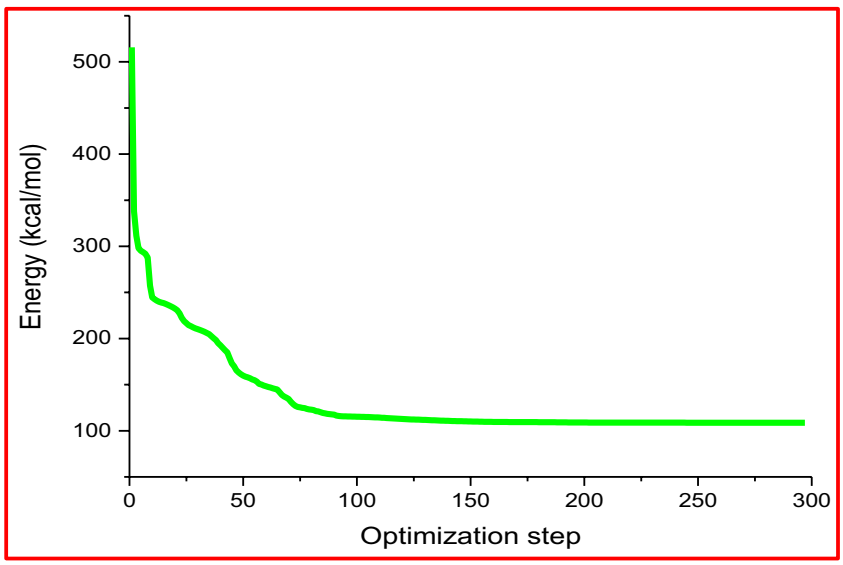

Fig. 16 Forcite geometry optimization of energy (*Amberlite*™ *IRC-200* resin molecule)

Table 8 Experimental inhibition efficiencies, the outputs, and descriptors calculated by the Monte Carlo simulation for adsorption of *Amberlite*™ *IRC-200* resin molecule on Fe(110) and Ni(110) (in kcal mol^{-1})

Inhibitor	Total energy	Adsorption energy	Rigid adsorption energy	Deformation energy	dE_{ad}/dN_i
Fe(110)	−164.17	−200.33	−129.32	−71.00	−200.33
Ni(110)	−110.97	−147.13	−73.41	−73.71	−147.13

for electrophile (f_r^-) and nucleophilic attacks (f_r^+), as well as their dual descriptors (f_r^2) of the *Amberlite*™ *IRC-200* resin at B3LYP/6–311 + G(d,p) in the PCM solvation model, while the numerical results are shown in Table 8.

For protonated form, the highest values for the condensed Fukui indices for electrophilic (f_r^-) are arranged as follows: C3 > C6 > C5, while those that are favored by the nucleophilic attacks (f_r^+) are as follows: C6 > C2 > C3.

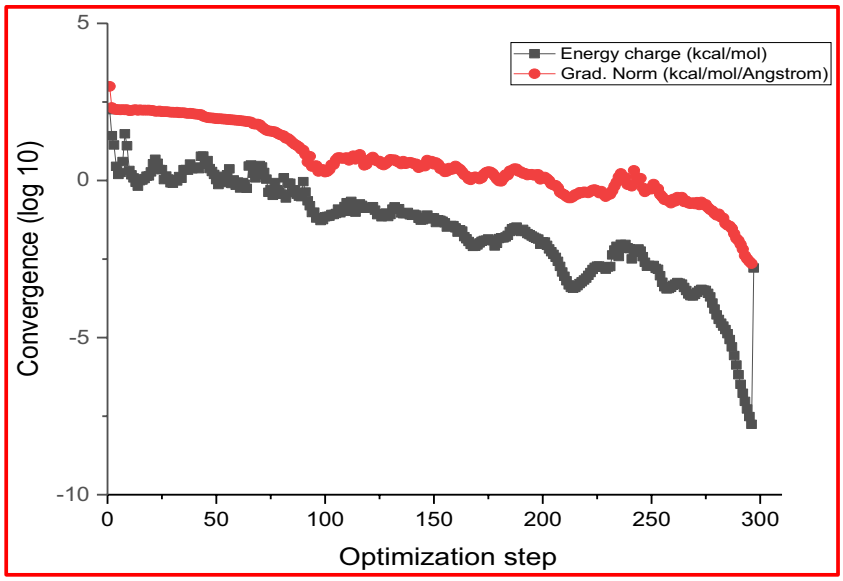

Fig. 17 Forcite geometry optimization of convergence (***Amberlite™ IRC-200*** resin molecule)

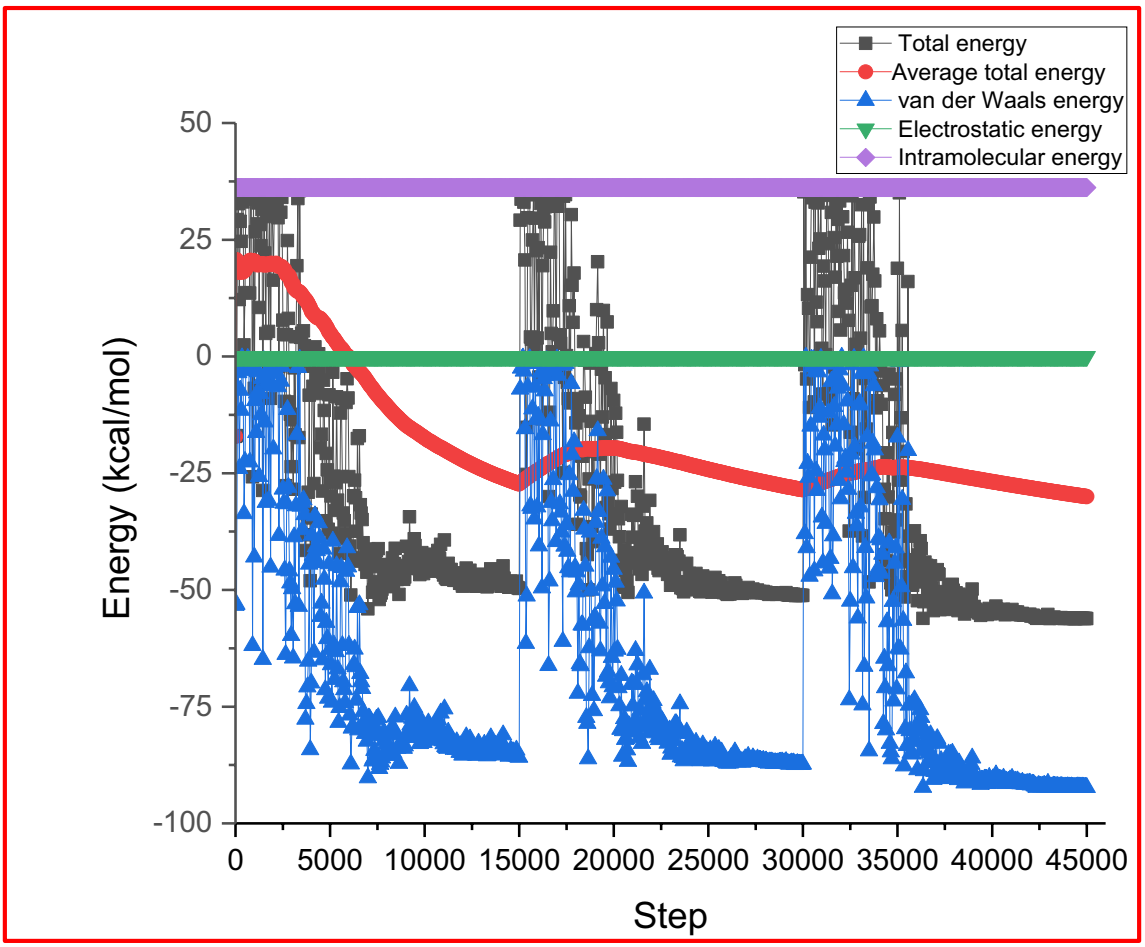

Fig. 18 The total energy change values between the molecule and Fe (110)

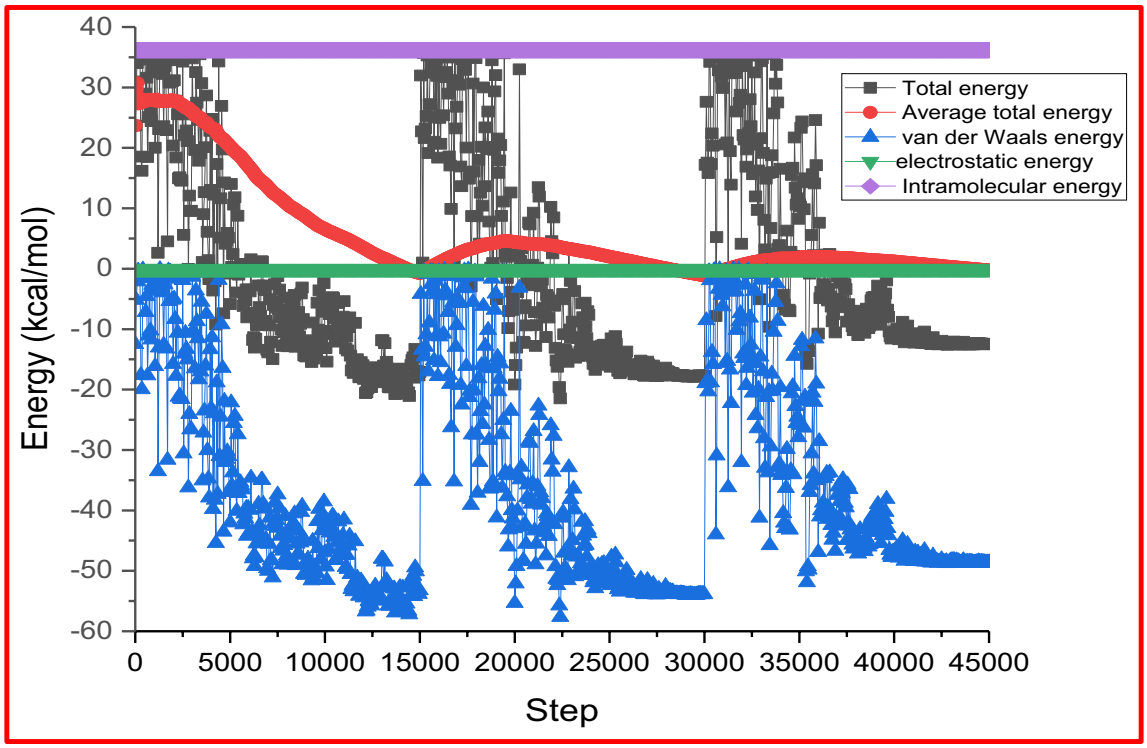

Fig. 19 The total energy change values between the molecule and Ni (110)

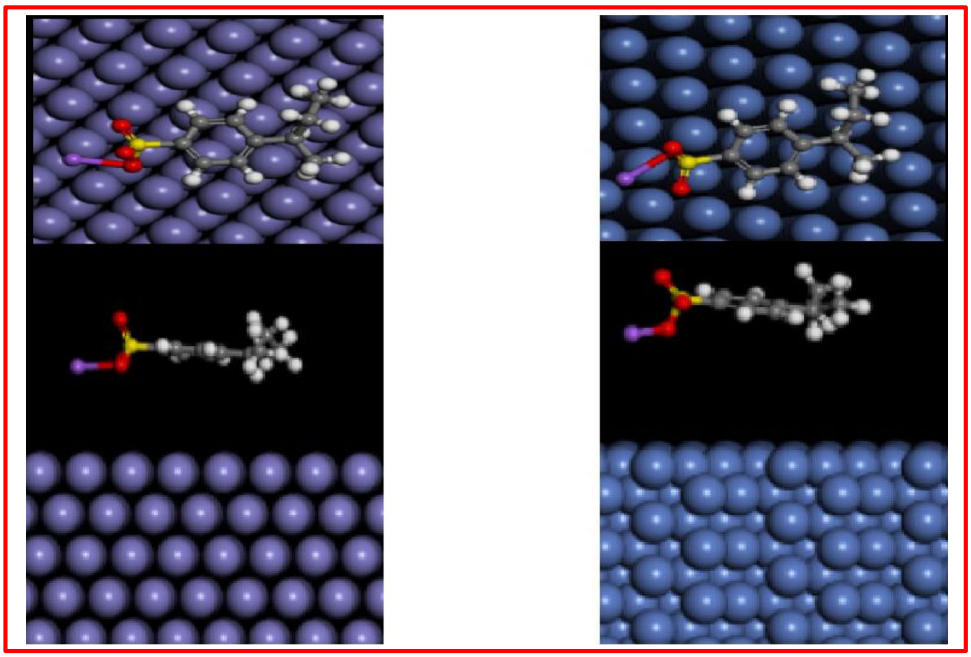

Fig. 20 Equilibrium adsorption of *Amberlite*™ *IRC-200* resin molecule on Fe(110) and Ni(110) surfaces obtained by simulation of molecular dynamics (upper panels: lateral views; lower panels: upper views)

On the other hand, for the anion form, the sites that are favored by electrophilic (f_r^-) are as follows: O12 > C3 > C6, while those that are responsible for nucleophilic attacks are arranged as follows: C1 > C4 > C2. For more accurate results, the dual Fukui descriptor is considered. The sites associated with $f_r^2 < 0$ correspond to the sites that are responsible for attacks nucleophilic, while those sites that are associated with $f_r^2 > 0$ are responsible for attacks electrophilic. For anion species, the data in Fig. 16 and Table 8 of the supplementary materials indicates that the most positive values occur at C4 and C2 of the phenyl group, suggesting that they are the most unfavorable sites for electrophilic

attack, whereas O12, C6, and C4 have large negative values and are hence favored by electrophilic reactants. For the protonated forms (Fig. 15b), it is clearly observed that the C1 and C3 have the most negative values and are hence favored by nucleophilic attacks, while the S7 and C2 sites have the most positive value and therefore favored by electrophilic attacks.

Molecular dynamic

Monte Carlo simulations are known to help predict the interaction between the inhibitor molecule and the metal surface (Dagdag et al. 2020). Figure 17 shows the optimization of the Forcite geometry for energy.

It is seen that the energy change gradually decreases with the increase of the optimization steps. At first, the energy tends to be minimized due to the instability of the molecular structure formula, while in the later stage, the total energy tends to be fixed with the optimization of the energy in Fig. 18.

Figure 19 shows the relation curve between the optimization of the convergence of the Forcite geometry and the number of optimization steps. Using the conjugate gradient optimization method and the molecular structure formula treatment, the figure shows that the energy and gradient values change gradually. Decreased with increasing stages of optimization, and then progressively, is due to the fact that the molecular structure formula progressively supplements the crystallization growth in the state of crystallization at low temperature (Dagdag et al. 2020).

In Fig. 20, the most stable low-energy adsorption configurations (1:1 ratio) of *Amberlite™ IRC-200* resin molecule with various metal surfaces during the energy optimization process were induced by Monte Carlo simulation. Outputs and descriptors, including total adsorption, rigid adsorption, and strain energies, are given in Table 8. The energy released during the relaxation of adsorbate components that are adsorbed on the substrate is what determines the adsorption energy (Tomasi et al. 2005).

The energy needed for adsorption is the combination of solid and deformation energy of the adsorbate component in the system. The more negative the adsorption energies are, the stronger the interaction between a metal and an inhibitory molecule. From the results in Table 8, it is seen that the negative values of the adsorption energies of *Amberlite™ IRC-200* resin molecule on different metal surfaces increase in the order of Ni(110) > Fe(110).

Conclusion

The aim of this study is to compare two washed and unwashed stages of the organic cationic molecule adsorbent resin (*Amberlite™ IRC-200*) which was the subject of this work. Both *Amberlite™ IRC-200* compounds act as inhibitors efficient for MS corrosive study in solution 1.0 M solution HCl acid, of which *Amberlite™ IRC-200* is a better inhibitor. Based on the obtained outcomes in this work, the efficiencies inhibition of the adsorbent *Amberlite™ IRC-200* washed and unwashed followed the order: 89.0% (washed) < 94.0% (unwashed) and their adsorption technical process. The coupled inductively spectroscopy technically (ICP) discloses that the efficacy inhibition increases with the diminution in the various concentration studies of the metal Fe^{2+} in the solutions inhibited. The DFT simulation also provides more information regarding the energy characteristics and reactivity of the inhibitory resin-iron region interaction. The results from the MC and MD analyses show that the inhibitory resin is most effective at interacting with oxygen heteroatoms because of its somewhat flat-adsorbed configuration on the resin's side walls. Data acquired from experiments provide support to the idea that inhibitory resin has significant negative adsorption energies. Moreover, furthermore, experimental techniques were supported by theory party DFT and simulation MC.

Acknowledgements 1. The authors thank the University Center for Analysis, Technology and Incubation Transfer Expertise (CUAE2TI), under the Ibn Tofaïl University of Kenitra.

2. The National Center for Scientific and Technical Research CNRST of Morocco has made available to the scientific equipment of the UATRS division.

3. Nuha Wazzan gratefully acknowledges King Abdulaziz University's High-Performance Computing Centre (Aziz Supercomputer) (http://hpc.kau.edu.sa) for assisting with the calculations for the work of this paper. A generous allocation of computing time at the CCC of the UAM is also acknowledged.

Author contribution Conceptualization, writing the original draft, reviewing, and editing: Jaouad Bensalah; formal analysis, funding acquisition, reviewing, and editing: Abdelfettah Hmada, Said Bouzakraoui, Nadia Dkhireche, Abdelkader Zarrouk, Şaban Erdoğan, Burak Tüzün; investigations: Nuha Wazzan, Zaki S. Safi, Hamid Erramli; resources, data validation, data curation, supervision, data: Mohamed Ebn Touhami and Amar Habsaoui.

Data availability Data is available throughout the manuscript and supporting files.

Declarations

Ethics approval and consent to participate Not applicable.

Consent for publication Not applicable.

Competing interests The authors declare no competing interests.

References

Abiola OK, Tobun Y (2010) Cocos nucifera L. water as green corrosion inhibitor for acid corrosion of aluminium in HCl solution. Chin Chem Lett 21:1449–1452. https://doi.org/10.1016/j.cclet.2010.07.008

Amri AE, Bensalah J, Idrissi A, Kadiri L, Ouass A, Bouzakraoui S, Zarrouk A, Rifi EH, Lebkiri A (2022) Adsorption of a cationic dye

(Methylene bleu) by Typha Latifolia: equilibrium, kinetic, thermodynamic and DFT calculations. Chem Data Collect 38:100834. https://doi.org/10.1016/j.cdc.2022.100834

Asan A, Soylu S, Kıyak T, Yıldırım F, Öztaş SG, Ancın N, Kabasakaloğlu M (2006) Investigation on some Schiff bases as corrosion inhibitors for mild steel. Corros Sci 48:3933–3944. https://doi.org/10.1016/j.corsci.2006.04.011

Becke AD (1988) Density-functional exchange-energy approximation with correct asymptotic behavior. Phys Rev A 38:3098–3100. https://doi.org/10.1103/PhysRevA.38.3098

Behpour M, Ghoreishi SM, Soltani N, Salavati-Niasari M, Hamadanian M, Gandomi A (2008) Electrochemical and theoretical investigation on the corrosion inhibition of mild steel by thiosalicylaldehyde derivatives in hydrochloric acid solution. Corros Sci 50:2172–2181. https://doi.org/10.1016/j.corsci.2008.06.020

Ben Hmamou D, Salghi R, Zarrouk A, Zarrok H, Al-Deyab SS, Benali O, Hammouti B (2012) The inhibited effect of phenolphthalein towards the corrosion of C38 steel in hydrochloric acid. Int J Electrochem Sci 7:8988–9003

Bensalah J, Benhiba F, Habsaoui A, Ouass A, Zarrouk A, Lebkiri A, El Khattabi O, Rifi EH (2022) The adsorption mechanism of the anionic and cationic dyes of the cationic resin A®IRC-50, kinetic study and theoretical investigation using DFT. J Indian Chem Soc 7:100512. https://doi.org/10.1016/j.jics.2022.100512

Bensalah J, Galai M, Ouakki M, El'Amri A, Boussfiha H, Habsaoui A, El Khattabi O, Lebkiri A, Zarrouk A, Rifi EH (2023a) A combined experimental and thermodynamics study of mild steel corrosion inhibition in 1.0 M hydrochloric solution by the cationic polymer Amberlite®IRC-50 resin extract. Chem Data Collect 43:100976. https://doi.org/10.1016/j.cdc.2022.100976

Bensalah J, Idrissi A, El Faydy M, Doumane G, Staoui A, Hsissou R, Lebkiri A, Habsaoui A, Zarrouk A, Rifi EH (2023b) Investigation of the cationic resin as a potential adsorbent to remove MR and CV dyes: kinetic, equilibrium isotherms studies and DFT calculations. J Mol Struct 1278:134849. https://doi.org/10.1016/j.molstruc.2022.134849

Bentiss F, Traisnel M, Vezin H, Lagrenée M (2003) Linear resistance model of the inhibition mechanism of steel in HCl by triazole and oxadiazole derivatives: structure–activity correlations. Corros Sci 45:371–380. https://doi.org/10.1016/S0010-938X(02)00102-6

Cruz J, Martínez R, García-Ochoa J, Garchoa E (2004) Experimental and theoretical study of 1-(2-ethylamino)-2-methylimidazoline as an inhibitor of carbon steel corrosion in acid media. J Electroanal Chem 566:111–121. https://doi.org/10.1016/j.jelechem.2003.11.018

Dagdag O, Berisha A, Safi Z, Dagdag S, Berrani M, Jodeh S, Verma C, Ebenso EE, Wazzan N, El Harfi A (2020) Highly durable macromolecular epoxy resin as anticorrosive coating material for carbon steel in 3% NaCl: computational supported experimental studies. J Appl Polym Sci 137:49003. https://doi.org/10.1002/app.49003

Dane F, Liu J, Zhang C (2007) Phylogeography of the bitter apple, Citrullus colocynthis. Genet Resour Crop Evol 54:327–336. https://doi.org/10.1007/s10722-005-4897-2

De Proft F, Martin JML, Geerlings P (1996) Calculation of molecular electrostatic potentials and Fukui functions using density functional methods. Chin Chem Lett 256:400–408. https://doi.org/10.1016/0009-2614(96)00469-1

Dkhireche N, Galai M, Kacimi YE, Rbaa M, Ouakki M, Lakhrissi B, Ebn Touhami M (2018) New quinoline derivatives as sulfuric acid inhibitor's for mild steel. Anal. Bioanal. Electrochem. 10: 11 1 - 1 3 5

Doumane G, Bensalah J, Hmada A, Iraqi O, Boussalem O, Mhanni D, Rifi EH, Safi ZS, Zarrouk A, Dkhireche N, Habsaoui A (2023) Corrosion inhibition performance of citrullus colocynthis seed oil extract as a mild steel in 1.0 M HCl acid using various solvants such as petroleum ether (CSOP) and cyclohexan (CSOC) polymerics. Inorg Chem Commun 155:111042. https://doi.org/10.1016/j.inoche.2023.111042

Eidi S, Azadi HG, Rahbar N, Mehmannavaz HR (2015) Evaluation of antifungal activity of hydroalcoholic extracts of Citrullus colocynthis fruit. J Herbal Med 5:36–40. https://doi.org/10.1016/j.hermed.2015.01.003

El Kerdoudi Z, Bensalah J, Ferraa N et al (2023) Physicochemical characterization of clay and study of cationic Methylene Blue dye adsorption. ACS Omega/. https://doi.org/10.1021/acsomega.3c06019

ElBelghiti M, Karzazi Y, Dafali A, Hammouti B, Bentiss F, Obot IB, Bahadur I, Ebenso EE (2016) Experimental, quantum chemical and Monte Carlo simulation studies of 3,5- disubstituted-4-amino-1,2,4-triazoles as corrosion inhibitors on mild steel in acidic medium. J Mol Liq 218:281–293. https://doi.org/10.1016/j.molliq.2016.01.076

Fuikui K (1982) Role of frontier orbitals in chemical reactions. 218:Science. 218:4574

Geethanjali R, Subhashini S (2015) Thermodynamic characterization of metal dissolution and adsorption of polyvinyl alcohol-grafted poly(acrylamide-vinyl sulfonate) on mild steel in hydrochloric acid: Port Electrochim Acta 33:35–48. https://doi.org/10.4152/pea.201501035

Ghazoui A, Zarrouk A, Bencaht N, Salghi R, Assouag M, El Hezzat M, Guenbour A, Hammouti B (2014) New possibility of mild steel corrosion inhibition by organic heterocyclic compound. J Chem Pharm Res 6(2):704–712

Hegazy MA, Abdallah M, Awad MK, Rezk M (2014) Three novel di-quaternary ammonium salts as corrosion inhibitors for API X65 steel pipeline in acidic solution. Part i: Exp Results Corros Sci 81:54–64. https://doi.org/10.1016/j.corsci.2013.12.010

Ho MX, Hudson BP, Das K, Arnold E, Ebright RH (2009) Structures of RNA polymerase–antibiotic complexes. Curr Opin Struct Biol 19:715–723. https://doi.org/10.1016/j.sbi.2009.10.010

Hsissou R, Abbout S, Benhiba F, Seghiri R, Safi Z, Kaya S, Briche S, Serdaroğlu G, Erramli H, Elbachiri A, Zarrouk A, El Harfi V (2021) Insight into the corrosion inhibition of novel macromolecular epoxy resin as highly efficient inhibitor for carbon steel in acidic mediums: synthesis, characterization, electrochemical techniques, AFM/UV–Visible and computational investigations. J Mol Liq 337:116492. https://doi.org/10.1016/j.molliq.2021.116492

Hu Z, Meng Y, Ma X, Zhu H, Li J, Li C, Cao D (2016) Experimental and theoretical studies of benzothiazole derivatives as corrosion inhibitors for carbon steel in 1 M HCl. Corros Sci 112:563–575. https://doi.org/10.1016/j.corsci.2016.08.012

Issa RM, Awad MK, Atlam FM (2010) DFT theoretical studies of antipyrine Schiff bases as corrosion inhibitors. Mater Corros 61:709–714. https://doi.org/10.1002/maco.200905361

Jiménez-Sánchez R, Pérez-Figueroa SE, Trejo-Baños A, Miranda Á, Salazar F, Cruz-Irisson M (2023) Surface Li effects on the electronic properties of GaAs nanowires: a first principles approach. Surf Interfaces 38:102745. https://doi.org/10.1016/j.surfin.2023.102745

Kadiri L, Galai M, Ouakki M, Essaaadaoui Y, Ouass A, Cherkaoui M, Rifi EH, Lebkiri A (2018) Coriandrum sativum L seeds extract as a novel green corrosion inhibitor for mild steel in 1.0 M hydrochloric and 0.5 M sulfuric solutions. Anal Bioanal Electrochem 10:249–268

Kayadibi F, Zor S, Sagdinc SG (2016) Experimental and theoretical evaluation of the inhibition properties of ketoprofen for the corrosion of a copper surface in hydrochloric acid. Prot Met Phys Chem Surf 52:356–371. https://doi.org/10.1134/S2070205116020131

Khaled K (2003) The inhibition of benzimidazole derivatives on corrosion of iron in 1 M HCl solutions. Electrochim Acta 48(17):2493–2503. https://doi.org/10.1016/S0013-4686(03)00291-3

Kouadri I, Layachi A, Makhlouf A, Satha H (2018) Optimization of extraction process and characterization of water-soluble polysaccharide (Galactomannan) from Algerian biomass; Citrullus colocynthis seeds. Int J Polym Anal Charact 23:362–375. https://doi.org/10.1080/1023666X.2018.1455343

Krishnegowda PM, Venkatesha VT, Krishnegowda PKM, Shivayogiraju SB (2013) Acalypha torta leaf extract as green corrosion inhibitor for mild steel in hydrochloric acid solution. Ind Eng Chem Res 52:722–728. https://doi.org/10.1021/ie3018862

Li X, Deng S, Fu H (2011) Triazolyl blue tetrazolium bromide as a novel corrosion inhibitor for steel in HCl and H2SO4 solutions. Corros Sci 53:302–309. https://doi.org/10.1016/j.corsci.2010.09.036

Lu T, Chen F (2012) Multiwfn: a multifunctional wavefunction analyzer. J Comput Chem 33:580–592. https://doi.org/10.1002/jcc.22885

Murulana LC, Kabanda MM, Ebenso EE (2016) Investigation of the adsorption characteristics of some selected sulphonamide derivatives as corrosion inhibitors at mild steel/hydrochloric acid interface: experimental, quantum chemical and QSAR studies. J Mol Liq 215:763–779. https://doi.org/10.1016/j.molliq.2015.12.095

Naseri E, Hajisafari M, Kosari A, Talari M, Hosseinpour S, Davoodi A (2018) Inhibitive effect of clopidogrel as a green corrosion inhibitor for mild steel; statistical modeling and quantum Monte Carlo simulation studies. J Mol Liq 269:193–202. https://doi.org/10.1016/j.molliq.2018.08.050

Ouakki M, Galai M, Cherkaoui M, Rifi EH , Hatim Z (2020) Study on the corrosion inhibition of mild steel in two acidic mediums (HCl 1M and H2SO4 0.5M) containing apatite

Rouifi Z, Rbaa M, Benhiba F, Laabaissi T, Oudda H, Lakhrissi B, Guenbour A, Warad I, Zarrouk A (2020) Preparation and anticorrosion activity of novel 8-hydroxyquinoline derivative for carbon steel corrosion in HCl molar: computational and experimental analyses. J Mol Liq 307:112923. https://doi.org/10.1016/j.molliq.2020.112923

Schafferman D, Beharav A, Shabelsky E, Yaniv Z (1998) Evaluation of Citrullus colocynthis, a desert plant native in Israel, as a potential source of edible oil. J Arid Environ 40:431–439. https://doi.org/10.1006/jare.1998.0454

Sherif E-SM, Erasmus RM, Comins JD (2008) Inhibition of copper corrosion in acidic chloride pickling solutions by 5-(3-aminophenyl)-tetrazole as a corrosion inhibitor. Corros Sci 50:3439–3445. https://doi.org/10.1016/j.corsci.2008.10.002

Spoor W (2001) Zohary D, Hopf M (2000) Domestication of plants in the old world. 3rd edn. 316pp. New York: Oxford University Press. £19.95 (softback). Ann Botany 88:666. https://doi.org/10.1006/anbo.2001.1505

Tayebi H, Bourazmi H, Himmi B, Assyry AE, Ramli Y, Zarrouk A, Geunbour A, Hammouti B (2014) Combined electrochemical and quantum chemical study of new quinoxaline derivative as corrosion inhibitor for carbon steel in acidic media. Der Pharma Chem 6(5):220–234

Tomasi J, Mennucci B, Cammi R (2005) Quantum mechanical continuum solvation models. Chem Rev 105:2999–3094. https://doi.org/10.1021/cr9904009

Yadav DK, Quraishi MA, Maiti B (2012) Inhibition effect of some benzylidenes on mild steel in 1 M HCl: an experimental and theoretical correlation. Corros Sci 55:254–266. https://doi.org/10.1016/j.corsci.2011.10.030

Zarrouk A, Hammouti B, Zarrok H, Salghi R, Dafali A, Bazzi Lh, Bammou L, Al-Deyab SS (2012) Electrochemical impedance spectroscopy and weight loss study for new pyridazine derivative as inhibitor for copper in nitric acid. Der Pharma Chem 4(1):337–346

Zarrouk A, El Ouali I, Bouachrine M, Hammouti B, Ramli Y, Essassi EM, Warad I, Aouniti A, Salghi R (2013) Theoretical approach to the corrosion inhibition efficiency of some quinoxaline derivatives of steel in acid media using the DFT method. Res Chem Intermed 39:1125–1133. https://doi.org/10.1007/s11164-012-0671-1

Zhong R, Li H, Wang Y, Zhang Y, Zhou J, Wang T (2023) Removal of antibiotic resistance genes and pathogenicity in effluent from municipal wastewater treatment plant by plasma oxidation. Chem Eng J 454:140274. https://doi.org/10.1016/j.cej.2022.140274

Zhou T, Hou Y, Yang Z, Laffitte Z, Luo K, Luo X, Liao D, Tang X (2023) Reducing spatial resolution increased net primary productivity prediction of terrestrial ecosystems: a random forest approach. Sci Total Environ 897:165134. https://doi.org/10.1016/j.scitotenv.2023.165134